Competing effects of nitrogen deposition and ozone exposure on Northern hemispheric terrestrial carbon uptake and storage, 1850-2099

Martina Franz[1,2] and Sönke Zaehle[1,3]

[1]Biogeochemical Signals Department, Max Planck Institute for Biogeochemistry, Jena, Germany
[2]International Max Planck Research School (IMPRS) for Global Biogeochemical Cycles, Jena, Germany
[3]Michael Stifel Center Jena for Data-driven and Simulation Science, Jena, Germany

Correspondence: Martina Franz (mfranz@bgc-jena.mpg.de)

Abstract.

Tropospheric ozone (O_3) and nitrogen deposition affect vegetation growth and ~~thus~~ thereby the ability of the land biosphere to take up and store carbon. However, the magnitude of ~~this effect~~ these effects on the contemporary and future terrestrial carbon balance is insufficiently understood. Here, we apply an extended version of the O-CN terrestrial biosphere model that simulates the atmosphere to canopy transport of O_3, its surface and stomatal uptake, the O_3-induced leaf injury, as well as the ~~ozone-induced leaf injury~~coupled terrestrial carbon and nitrogen cycles. We use this model to simulate past and future impacts of air pollution ~~(ozone and nitrogen deposition)~~ against a background of concurrent changes in climate and carbon dioxide concentrations (CO_2) for two contrasting representative concentration pathways (RCP) scenarios (RCP2.6 and RCP8.5).

The simulations show that O_3-related damage considerably reduced Northern hemispheric gross primary production (GPP) and long-term carbon storage between 1850 and the 2010s. The ~~ozone~~ simulated O_3 effect on GPP in the Northern hemisphere ~~peaks at~~ peaked towards the end of the 20^{th} century with reductions of 4 %, causing a reduction in the Northern hemispheric carbon sink of 0.4 PgCyr^{-1}. During the 21^{st} century, ~~ozone-induced~~ O_3-induced reductions in GPP and carbon storage ~~is~~ are projected to decline through a combination of direct air pollution control methods that reduce ~~tropospheric~~ near surface O_3 and the indirect effects of rising atmospheric CO_2, which reduces stomatal uptake of ~~ozone~~ O_3 concurrent with increases of leaf-level water-use efficiency.

However, in hotspot regions such as East Asia, the model simulations suggest a sustained decrease of GPP by more than 8~~% during~~ % throughout the 21^{st} century. ~~Regionally, ozone exposure reduces~~ O_3 exposure reduces projected carbon storage at the end of the 21^{st} century by up to 15 % in parts of Europe, the US and East Asia. ~~These estimates are lower compared to previous studies, which partially results from the explicit representation of non-stomatal ozone destruction, which considerably reduces simulated ozone uptake by leaves and incurred injury.~~

Our simulations suggest that ~~ozone damage largely offsets the growth stimulating effect induced by nitrogen deposition in~~ the ~~Northern hemisphere until the 2050s. Thus, accounting~~ stimulating effect of nitrogen deposition on regional GPP and carbon storage is lower in magnitude compared to the detrimental effect of O_3 during most of the simulation period for both RCPs. In the second half of the 21^{st} century, the detrimental effect of O_3 on GPP is outweighed by nitrogen deposition, but the

effect of nitrogen deposition on land carbon storage remains lower than the effect of O_3. Accounting for the stimulating effects of nitrogen deposition but omitting the detrimental effect of O_3 ~~might~~ may lead to an over estimation of projected carbon uptake and storage.

1 Introduction

Productivity and carbon storage in many Northern hemispheric terrestrial ecosystems are affected by the limited availability of nitrogen ~~(Vitousek and Howarth, 1991; LeBauer and Treseder, 2008; Zaehle, 2013)~~(N; Vitousek and Howarth, 1991; LeBauer and Tresed . As a side-effect of air pollution, increased deposition of reactive nitrogen from e.g. anthropogenic fossil fuel burning and increased soil emissions associated with fertiliser use (Galloway et al., 2004) have the potential to fertilise these N-limited ecosystems and thereby enhance productivity and carbon storage (Norby, 1998; Zaehle et al., 2011; Thomas et al., 2010). However, oxidised forms of reactive nitrogen in the atmosphere (collectively referred to as NO_y) are also a precursor of tropospheric ozone (O_3). Ozone (O_3) is a toxic air pollutant that enters plants primarily though the leaves' stomata where it can induce cellular damage (Fiscus et al., 2005; Tausz et al., 2007; McAinsh et al., 2002). Commonly observed effects are visible injury (Langebartels et al., 1991; Wohlgemuth et al., 2002), reductions in photosynthetic capacity (Tjoelker et al., 1995; Wittig et al., 2007) ~~,~~ and growth or yield (Grantz et al., 2006; Hayes et al., 2007; Feng and Kobayashi, 2009; Wittig et al., 2009; Leisner and Ainsworth, 2012). Ozone induced plant damage can reduce the terrestrial carbon uptake and storage and through this cause an increase in atmospheric CO_2 concentrations and an intensification of climate change (Sitch et al., 2007; Ainsworth et al., 2012).

~~Ozone concentrations over the mid- and high-latitudes of Eurasia and North America~~ Ozone mixing ratios in Europe have approximately doubled ~~between the pre-industrial period (around 1860) and the year 2000 (Akimoto, 2003; Cooper et al., 2014; Marenco et al~~ during the 20^{th} century (Cooper et al., 2014). The anthropogenic increase in NO_y emissions primarily from combustion sources has been identified as the major cause for the increasing near-surface ~~ozone concentrations between 1970-1995~~ O_3 concentrations between 1970–1995 in the mid-latitudes of the Northern Hemisphere (Fusco and Logan, 2003). Ozone levels are projected to decline until the end of the 21^st century due to assumed stringent air pollution policies, but future climate conditions with increasing temperatures as well as reduced cloudiness and precipitation will tend to increase ~~ozone~~ O_3 formation with increasing daily ~~ozone~~ O_3 peaks and average concentrations in summer (Meleux et al., 2007; van Vuuren et al., 2011). The application of the RCP scenarios (Moss et al., 2010; van Vuuren et al., 2011) in 14 global chemistry transport models results in the projection of declining annual global mean surface O_3 concentrations in most regions of the globe except South Asia where increases are simulated (Wild et al., 2012). Projections of nitrogen deposition in the 21^{st} century suggest little change across all scenarios of the Representative concentration pathways (RCP), despite notable regional differences (Lamarque et al., 2013). ~~Only under the most optimistic scenario RCP2.6 a~~ A small decline in deposition rates is proposed only under the scenario RCP2.6.

Simulations with nitrogen-enabled terrestrial biosphere models suggest that N deposition may be responsible for 10 to 50 % of the global residual land carbon uptake (Zaehle et al., 2011; Quéré et al., 2018). Several models including the ~~ozone~~

O_3 effect on carbon cycle suggest that simulated present-day and future ~~ozone~~ O_3 exposure can reduce regional and global scale productivity (Felzer et al., 2005; Sitch et al., 2007; Franz et al., 2017; Lombardozzi et al., 2015; Oliver et al., 2018). For instance, modelling studies by Sitch et al. (2007) and Oliver et al. (2018) suggest a reduction in O_3 induced damage of ~~global~~ gross primary production (GPP) by ~~4-15~~ 4–15 % and an associated reduction of land carbon storage by ~~3-10 %.~~ 3–10 %. Where Sitch et al. (2007) simulated global O_3 impacts between 1901–2100 and Oliver et al. (2018) focused on a European scale damage between 1901–2050.

Here, we assess the combined effect of ~~ozone~~ O_3 and nitrogen deposition on the Northern hemispheric terrestrial biosphere against the background of simulated changes due to increasing atmospheric CO_2 and climate change. Elevated levels of atmospheric CO_2 stimulate leaf photosynthesis and reduce stomatal conductance (Medlyn et al., 2001; Ainsworth and Long, 2005), and therefore can increase plant growth and plant nitrogen limitation (Oren et al., 2001; Norby et al., 2009; Zaehle et al., 2014). However, reductions in stomatal conductance reduce the leaf-level uptake of air pollutants like O_3 and thereby have the potential to restrict ~~ozone~~ O_3 induced damage to plants (Paoletti and Grulke, 2005; Barnes and Pfirrmann, 1992; Isebrands et al., 2001; Talhelm et al., 2014; Zak et al., 2011; Noormets et al., 2010).

We analyse the response of the Northern hemispheric carbon cycle to changes in climate, atmospheric CO_2 and O_3 as well as N deposition for the historical period (~~1850-2005~~1850–2005) and two future scenarios (~~2006-2099), the most optimistic and most pessimistic RCP scenario~~(2006–2099), a high and a low climate-change mitigation scenario, RCP2.6 and RCP8.5 respectively~~)~~. In a factorial analysis, we investigate the impact of the single drivers (O_3, CO_2 and N deposition), as well as their interaction (specifically the interaction between O_3 and CO_2, and O_3 and N deposition) on plant growth and terrestrial carbon storage. We employ a significantly enhanced version of the O-CN terrestrial biosphere model (Zaehle and Friend, 2010), which explicitly accounts for the O_3 transport and deposition from the free ~~atmosphere into the stomates~~troposphere into the stomata, as well as ~~ozone uptake~~ O_3 removal by other processes (such as soil and leaf surface uptake) (Franz et al., 2017). This model has been evaluated against biomass damage relationships observed in a range of fumigation/filtration experiments with European tree species (Büker et al., 2015; Franz et al., 2018).

2 Methods

Simulations are conducted with the O-CN terrestrial biosphere model (Zaehle and Friend, 2010; Franz et al., 2017), version tun$_{VC}$ where ~~ozone~~ O_3 damage is calculated based on injury functions to the maximum carboxylation capacity of the leaf V_{cmax} (Franz et al., 2018). The tun$_{VC}$ injury functions were calibrated to reproduce observed biomass damage relationships of experiments with a range of European tree species in fumigation/filtration experiments ~~(Franz et al., 2018). Contrary to Franz et al. (2018),~~ (Franz et al., 2018; Büker et al., 2015).

The O-CN model includes an O_3 deposition scheme that explicitly accounts for the O_3 transport and deposition from the free troposphere into the stomata (Franz et al., 2017). Here, we use the ozone deposition scheme ~~described in Franz et al. (2017) is applied in the simulations here (~~referred to as D-model ~~version in Franz et al. (2017))~~in Franz et al. (2017), contrary to Franz et al. (2018) where the O_3 deposition scheme was turned off.

2.1 The O-CN model

O-CN (Zaehle and Friend, 2010) is a further development of the ~~biogeochemistry in the~~ land-surface-scheme ORCHIDEE (Krinner et al., 2005), and simulates the coupled terrestrial carbon (C), nitrogen (N) and water cycles for twelve plant functional types. The model accounts for the effects of nitrogen availability on growth, root:shoot allocation, litter and soil organic matter decay, and represents a comprehensive nitrogen cycle including process-oriented formulations for nitrogen leaching and gas losses, and its ability to reproduce N fertilisation experiments has been evaluated by (Meyerholt and Zaehle, 2015). O-CN compares well to a range of regional to global terrestrial biosphere benchmarks (Quéré et al., 2018). O-CN is driven by climate data, N deposition, atmospheric composition including the ~~deposition,~~ atmospheric CO_2 and O_3 ~~burden,~~ concentrations and land use information~~(land cover, land cover change, and fertiliser application)~~.

O-CN simulates a multi-layer canopy with up to 20 layers (each with a thickness of up to 0.5 leaf area index) where net photosynthesis is calculated for shaded and sun-lit leaves with consideration of the light profiles of diffuse and direct radiation (Kull and Kruijt, 1998; Friend, 2001; Zaehle and Friend, 2010). Stomatal conductance to water, CO_2 and O_3 is calculated coupled to net photosynthesis following a Ball-&-Berry-type formulation (see Sect. 2.2). Leaf nitrogen concentration and leaf area determine the photosynthetic capacity, which are both affected by ecosystem available N. The maximum carboxylation capacity (V_{cmax}) and electron transport capacity (J_{max}) of the leaf increase with an increased leaf nitrogen concentration, leading to an increase in the maximum net photosynthesis and stomatal conductance per unit leaf area (Zaehle and Friend, 2010). The highest leaf N content is simulated at the top of the canopy and exponentially decreases with increasing canopy depth (Friend, 2001; Niinemets et al., 2015). Following this, the net photosynthesis, stomatal conductance and O_3 uptake are generally highest in the top of the canopy and lowest in the bottom of the canopy. Changes in stomatal conductance affect transpiration rates and estimates of O_3 uptake and ~~ozone~~ O_3 damage.

2.2 Ozone injury calculation in O-CN

Leaf-level ~~ozone~~ O_3 uptake is determined by stomatal conductance and atmospheric O_3 concentrations, as described in Franz et al. (2017). In contrast to Franz et al. (2017), the stomatal conductance g_{st} is calculated based on the Ball and Berry formulation (Ball et al., 1987) as

$$g_{st,l} = g_0 + g_1 \times \cancel{\frac{A_{n,l} \times RH \times f(height_l)}{C_a}} \frac{A_{\mathrm{n},l} \times RH \times f(height_l)}{[CO_2]} \tag{1}$$

where ~~net photosynthesis ($A_{n,l}$)~~ RH is the atmospheric relative humidity, $f(height_l)$ the water-transport limitation with canopy height, $[CO_2]$ the atmospheric CO_2 concentration, $A_{\mathrm{n},l}$ the net photosynthesis, g_0 the residual conductance when A_n approaches zero, and g_1 the stomatal-slope parameter as in Krinner et al. (2005). The index l indicates that g_{st} and A_n are calculated separately for each canopy layer. $A_{\mathrm{n},l}$ is calculated as described in Zaehle and Friend (2010) as a function of the leaf-internal partial pressure of CO_2, absorbed photosynthetic photon flux density on shaded and sunlit leaves, leaf temperature, the nitrogen-specific rates of maximum light harvesting, electron transport (J_{max}) and carboxylation rates (V_{cmax}). ~~RH is the~~

~~atmospheric relative humidity, $f(height_l)$ the water-transport limitation with canopy height, C_a the atmospheric concentration, g_0 the residual conductance when A_n approaches zero, and g_1 the stomatal-slope parameter as in Krinner et al. (2005). The index l indicates that g_{st} is calculated separately for each canopy layer.~~

The stomatal conductance to ~~ozone~~ O_3 $g_{st,l}^{O_3}$ is calculated as

$$g_{st,l}^{O_3} = \frac{g_{st,l}}{1.51} \tag{2}$$

where the factor 1.51 accounts for the different diffusivity of O_3 from water vapour (Massman, 1998).

For each canopy layer, the O_3 stomatal flux ($f_{st,l}$, $\mathrm{nmol\,m^{-2}\,s^{-1}}$) is calculated from the canopy O_3 concentration ($\cancel{\chi_{can}^{O_3}}[O_3]^{can}$), and $g_{st,l}$ is calculated as

$$f_{st,l} = (\chi_{atm}^{O_3}[O_3]^{can} - \chi_i^{O_3}[O_3]^i)g_{st,l}^{O_3}. \tag{3}$$

where the leaf-internal O_3 concentration ($\cancel{\chi_i^{O_3}}[O_3]^i$) is assumed to be zero (Laisk et al., 1989).

The ~~ozone~~ O_3 deposition module calculates $\cancel{\chi_{can}^{O_3}}$ $[O_3]^{can}$ from the O_3 concentration in 45~~m height ($\chi_{atm}^{O_3}$)as provided by the chemical transport models as input for terrestrial biosphere models like O-CN (Franz et al., 2017). $\chi_{can}^{O_3}$, is calculated based~~ m height ($[O_3]^{atm}$), which represents the lowest level O_3 concentrations in the forcing data (Franz et al., 2017). Based on the constant flux assumption $[O_3]^{can}$ in units of $\mathrm{nmol\,m^{-3}}$ is calculated as

$$\chi_{can}^{O_3}[O_3]^{can} = \chi_{atm}^{O_3}[O_3]^{atm}(1 - \frac{R_a}{R_a + R_b + R_c}) \tag{4}$$

with R_a the aerodynamic resistance, R_b the canopy-scale quasi-laminar layer resistance and R_c the compound surface resistance to O_3 deposition. R_c is calculated as the sum of the canopy scale stomatal and the non-stomatal resistance to O_3 uptake (Franz et al., 2017). The non-stomatal resistance is defined by the O_3 destruction on the leaf surface, within-canopy resistance to O_3 transport, and ground surface resistance (Franz et al., 2017).

~~Part of the O_3 taken up into the leaves is assumed to get detoxified and to cause no damage to the plant. Ozone fluxes exceeding the detoxification threshold of X ($f_{st,l,X}$,) are accumulated over time to give the cumulative~~ Without the application of the O_3 ~~uptake above a flux~~ deposition module, the O_3 uptake inside the leaves would be calculated based on the near surface O_3 concentrations from the forcing data without accounting for the turbulent transport between the lower troposphere and the leaves, as well as the deposition and destruction of ozone on other surfaces.

The accumulation of O_3 fluxes into the leaves above a threshold of X $\mathrm{nmol\,m^{-2}\,s^{-1}}$ (~~$CUOX_l$) with~~ $f_{st,l,1}$, $\mathrm{nmol\,m^{-2}\,s^{-1}}$) with

$$f_{st,l,X}\,{}_{st,l}(X) = \cancel{MAX}\,max(0, f_{st,l} - X). \tag{5}$$

gives the $CUOX_l$. Summing $CUOX_l$ over all canopy layers gives the canopy value $CUOX$ (Franz et al., 2017). In this study, a flux threshold of $1\,\mathrm{nmol\,m^{-2}\,s^{-1}}$, i.e. CUO1, is applied to account for the plants ability to detoxify part of the taken up O_3 (Franz et al., 2018; LRTAP-Convention, 2017; Büker et al., 2015). The cumulative uptake of O_3 without detoxification, i.e. a threshold of zero, is represented by CUO0.

Emerging leaves are assumed undamaged and accumulate $CUOX$ during the growing season. The $CUOX_l$ is reduced by the fraction of newly developed leaves per time step and canopy layer. Deciduous PFTs shed all $CUOX$ at the end of the growing season and grow uninjured leaves the next spring. Evergreen PFTs shed proportionate amounts of $CUOX$ during the entire year when new leaves or needles are grown or old foliage is replaced.

The ~~ozone~~ O_3 injury fraction ($d_l^{O_3}$), is calculated as a linear function of $CUO1_l$

$$d_l^{O_3} = 1 - b \times CUO1_l \tag{6}$$

where the slope of the injury function (b) is set to 0.075 for broadleaf species and 0.025 for needleleaf species (Franz et al., 2018). $d_l^{O_3}$ is calculated separately for each canopy layer l according to the specific accumulated ~~ozone~~ O_3 uptake of the respective canopy layer ($CUO1_l$), and takes values between 0 and 1. Within-canopy gradients in stomatal conductance and photosynthetic capacity cause variations of $CUO1_l$ and hence $d_l^{O_3}$ between canopy layers.

The effect of ~~ozone~~ O_3 injury on plant carbon uptake is calculated by

$$V_{cmax,l}^{O_3} = V_{cmax,l}(1 - d_l^{O_3}). \tag{7}$$

with the maximum carboxylation capacity of the leaf in the respective canopy layer ($V_{cmax,l}$), which is used in the calculation of $\cancel{A_{n,t}}$ $A_{\mathrm{n},l}$. $\mathrm{J}_{max,l}$ is reduced in proportion to $V_{cmax,l}$ such that the ratio between both ~~keeps~~ is maintained.

Ozone induced reductions in $\cancel{A_{n,t}}$ $A_{\mathrm{n},l}$ cause a decline in $g_{st,l}$ as both are tightly coupled. Lower values of $g_{st,l}$ diminish the O_3 uptake into the plant ($f_{st,l}$) and slow the increase in $CUO1_l$ and hence ~~ozone~~ O_3 induced injury.

2.3 Model forcing

The model is driven by climate model output of the Institute Pierre Simon Laplace (IPSL) general circulation model IPSL-CM5A-LR (Dufresne et al., 2013), bias-corrected according to the Inter-Sectoral Impact Model Intercomparison Project (Hempel et al., 2013). ~~Downward nitrogen deposition velocity and near surface ozone~~ The applied meteorological forcing for near-surface conditions comprises daily data of specific humidity, incoming long wave radiation, incoming short wave radiation, cloudiness, wind speed, maximum temperature, minimum temperature and total precipitation, which are disaggregated to the 30 min time step of the model using a statistical weather generator (Krinner et al., 2005). Reduced and oxidised monthly mean nitrogen deposition in wet and dry form and monthly mean near surface O_3 concentrations are provided by CAM, the community atmosphere model (Lamarque et al., 2010; Cionni et al., 2011). Land cover, soil, and N fertiliser application are used as in Zaehle et al. (2011) and kept at 2000 values throughout the simulation. Data on atmospheric CO_2 concentrations are obtained from Meinshausen et al. (2011). Through all simulations present day land-use information are applied for the year 2000 (Hurtt et al., 2011).

Figure 1 provides and overview over the scenarios applied in this study. Note that there are important regional patterns behind the changes in N deposition and ~~tropospheric ozone~~near surface O_3, which are shown in the ~~Appendix~~ Supplement Fig. S1 and ~~Fig.~~ S2.

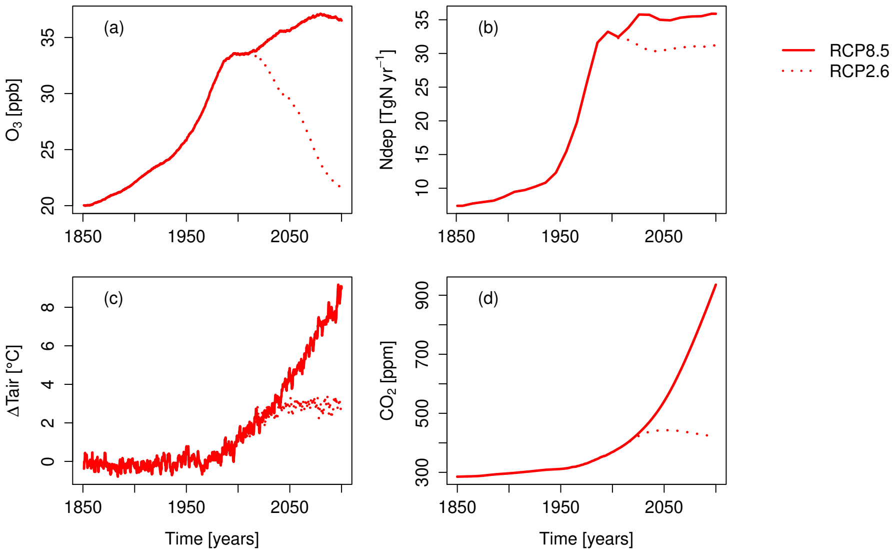

Figure 1. Time series of the terrestrial Northern hemispheric ($\geq$ 30°N) ~~)~~ mean a) ~~tropospheric ozone~~ near surface O_3 concentration, b) summed nitrogen deposition, c) air temperature at 2 m height, and d) atmospheric CO_2 concentration according to the RCP2.6 and RCP8.5 ~~pollution~~ emission scenario. For visual clarity, the effect of the seasonal cycles of ~~tropospheric ozone~~ near surface O_3 and N deposition are smoothed by a moving average of 12 months. See SI for spatial patterns of N deposition and ~~tropospheric ozone~~ near surface O_3 (~~Appendix~~ Supplement Fig. S1 and Fig. S2).

2.4 Modelling protocol

The model is run at a spatial resolution of 1° ~~x~~ × 1° and operates on a half hourly time step. As the injury functions developed by Franz et al. (2018) are based on ~~manipulation~~ exposure experiments with boreal and temperate European tree species, the simulation ~~scope~~ domain is restricted to the temperate and boreal region of the Northern Hemisphere $\geq$ 30°N.

To achieve an equilibrium in terms of the terrestrial vegetation and soil carbon and nitrogen pools, O-CN is run for 1291 years (including 10 iterations of 1000 years soil biogeochemistry and 100 years vegetation+soil biogeochemistry) by using the forcing data of the year 1850 data. Prior to year 1901 climate years are randomly iterated from the period of 1901 to 1930, as 1901 is the first year of the climate data set.

From this equilibrium, five factorial simulation runs are simulated where key drivers of plant growth and carbon sequestration (CO_2, climate, nitrogen deposition, O_3) are simulated either as fixed to the reference year, or transient (i.e. progressively changing within the simulation period) (see Tab. 1). These simulations run from the year 1850 to 2099. The period up to the

Table 1. Forcing setting of the factorial runs. Climate forcing for the years prior to 1901 is always drawn from the same random sequence of years between 1901 and 1930.

Factorial run	CO_2	Climate	Nitrogen deposition	O_3
S1	~~1850-2099~~ 1850–2099	~~1901-1930~~ 1901–1930	1850	1850
S2	~~1850-2099~~ 1850–2099	~~1901-1930~~ 1901–1930	1850	~~1850-2099~~ 1850–2099
S3	~~1850-2099~~ 1850–2099	~~1901-2099~~ 1901–2099	1850	~~1850-2099~~ 1850–2099
S4	~~1850-2099~~ 1850–2099	~~1901-2099~~ 1901–2099	~~1850-2099~~ 1850–2099	1850
S5	~~1850-2099~~ 1850–2099	~~1901-2099~~ 1901–2099	~~1850-2099~~ 1850–2099	~~1850-2099~~ 1850–2099

year 2005 is simulated identical for both ~~RCPs~~RCP scenarios. From 2006 until 2099 simulations are run using the forcing according to either the RCP2.6 or the RCP8.5 forcing scenario (Moss et al., 2010; van Vuuren et al., 2011).

To investigate the impact of the ~~ozone~~ O_3 deposition scheme on the simulation results, the factorial runs are repeated with a model version where the ~~ozone~~ O_3 deposition scheme is turned off (see ATM model version in (Franz et al., 2017). In simulations where the ~~ozone~~ O_3 deposition module is turned ~~,~~ off the canopy ~~ozone~~ O_3 concentration equals the O_3 concentration at 45 m above the surface which is the hight of the lowest level of the ~~atmospheric chemistry transport model (CTM) that deliver the forcing for our runs here~~forcing data.

2.5 Factorial analysis

The impact of a single forcing driver on the simulation results can be approximated by subtracting the simulation results of suitable combination of factorial runs from one another (see Tab.2). In the following, the term 'forcing driver' is used to refer to the input variables of the conducted simulations and 'single driver' refers to the approximated impact of a single forcing driver on the simulation results. The described approach is an approximation of the impact of the single drivers and assumes that the ~~drivers effect~~ effects on the analysed output variables ~~is~~ are additive. The assumption of additive effects is a necessary simplification to restrict the number of simulations and computation time (Zaehle et al., 2010). For O_3, a main driver of interest, two different approaches to calculate the single driver were realised. In one approach, the O_3 impact is calculated from the two factorial runs with only one/ two transient drivers (S1 and S2), and a second time from the factorial runs where all and all but one driver (S5 and S4 respectively) are simulated transient. The comparison of these two approaches to calculate the single driver might indicate the ~~extend~~ extent of impact of interacting forcing drivers on the estimate of the O_3 single driver. The relative changes between two simulation runs SX and SY are calculated as $(SX - SY)/SY$.

3 Results

The simulations show a strong increase in gross primary production (GPP) in the Northern Hemisphere ($\geq 30°$N) between the year 1850 and 2099 with all forcings considered in this study (S5; Fig. 2). ~~There is a notable difference between the scenarios,~~

Table 2. Calculation of the single driver effects (CO_2, climate, nitrogen deposition, O_3) from the conducted simulations. $S1_{ref}$ refers to the mean of the years 1850 to 1859 of the S1 simulation. ~~The relative changes between simulation SX and SY reported in Section 3 are calculated as $(SX - SY)/SY$~~ See Tab. 1 for info on the forcing setting of the factorial runs S1–S5.

Attributed single driver	Simulations
CO_2	$S1 - S1_{ref}$
O_3 approach 1	$S2 - S1$
O_3 approach 2	$S5 - S4$
Climate	$S3 - S2$
Nitrogen deposition	$S5 - S3$

~~with smaller simulated changes for the RCP 2.6 scenario, which level of at an increase by about a third. GPP continues to increase~~ In simulations based on the RCP8.5 scenario, GPP increases throughout the 21^st century~~under the RCP 8.5 scenario~~, roughly doubling by the year 2099 relative to 1850 values~~by the year 2099. Reflecting the changes in productivity,~~ . In the RCP 2.6 scenario, the simulated increase in GPP levels off in the 2040s at approximately a third of the simulated increase at the end of the 21^{st} century in the RCP8.5 scenario. The changes in terrestrial carbon storage ~~also increases~~ reflect these changes in GPP (see Fig. 2d).

Concurrent with the strong increase in GPP is an increased foliar uptake of ~~ozone~~O_3, which parallels the increase in ~~tropospheric~~ near surface and canopy-air O_3 concentrations (Fig.3). Simulated changes in the cumulative O_3 uptake without a flux threshold (CUO0, see Methods) strongly follow changes in the O_3 concentrations during the entire simulation period. Accounting for the ability of leaves to detoxify part of the ~~ozone~~ O_3 taken up, the cumulative canopy O_3 uptake above a flux threshold of $1\,\mathrm{nmol\,m^{-2}\,s^{-1}}$ (CUO1) does not remain at ~~relative~~ relatively constant values during the 21^{st} century under RCP8.5. Instead, it reaches a maximum at the end of the 20^{th} century and steadily declines afterwards. This difference between CUO0 and CUO1 for simulations based on RCP8.5 implies that the frequency at which the detoxification threshold is exceed gradually declines during the 21^{st} century. This results from a decline in peak uptake rates (F_{st}) in the 21^{st} century (Fig.3b) despite fairly constant ~~tropospheric~~ near surface O_3 concentrations (Fig.3a). The decline in peak uptake rates is the consequence of the reduced ratio of stomatal conductance to net photosynthesis under high atmospheric CO_2.

3.1 Factorial Analysis

We next decompose the simulations into the effects of the different model drivers with a special focus on the effects of ~~O_3~~ O_3 and nitrogen deposition. In all five factorial runs the simulated GPP increases strongly between 1850 and 2099 and approximately doubles for the run S5 based on RCP8.5 (see Fig. 2a). The primary cause for this simulated increase is the CO_2 fertilisation effect induced by increasing atmospheric CO_2 concentrations (see Fig. 4c and Tab. 3). Climate change is the second most ~~import~~ important factor for the simulated increase, whereas the positive effect of N deposition is less pronounced. Ozone injury causes a modest decrease in productivity, which manifests strongest during the 1990s. During the 20^{th} century

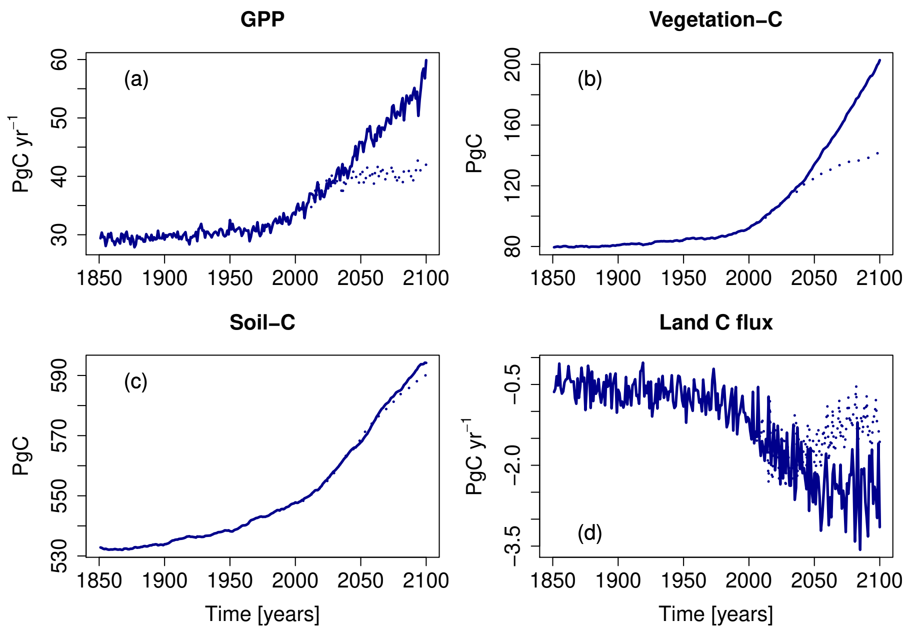

Figure 2. Simulated Northern hemispheric gross primary production (GPP), vegetation carbon (vegetation-C), soil carbon, and net land C flux of the factorial run S5 (all variables are simulated transient, see Tab. 1). Displayed are the period of ~~1850-2099~~ 1850–2099 for both the RCP2.6 and RCP8.5. See also Tab. 3.

the decline gradually reverses. The land carbon sink strongly responds to elevated levels of CO_2 (see Fig. 4f), whereas climate change induces a varying impact on the land carbon sink. During the second half of the 21^{st} century, the effect of climate mainly causes a reduction in the simulated land carbon sink.

3.2 Magnitude of nitrogen deposition impact

Nitrogen deposition has a positive effect on the simulated carbon uptake, storage and ~~ozone~~ O_3 uptake and accumulation in plants, but the magnitude varies between the different scenarios. N deposition ~~increases simulated~~ increased summed regional GPP by about 2.1 % (0.7 $\mathrm{PgC\,yr^{-1}}$) ~~in the present~~ at the beginning of the 21^{st} century compared to pre-industrial values (see Fig. 5, ~~Appendix~~ Supplement Fig. S3, and Tab. ~~??~~4). At the end of the 21^{st} century, GPP is increased by approximately 2.5 % under both RCPs.

Carbon stored in vegetation (vegetation-C) is increased by nitrogen deposition by about 2 % (2.1 PgC) ~~in the present~~ at the beginning of the 21^{st} century and by approximately 3 % (4.4 ~~-6.1~~ and 6.1 $\mathrm{PgC\,yr^{-1}}$ for RCP2.6 and RCP8.5 respectively) at the end of the 21^{st} century. This positive effect of N deposition keeps growing in ~~China~~ East Asia until the of the 21^{st} century (see Tab. ~~??). However,~~ 4), whereas in Europe and the ~~USA~~temperate North America, the GPP and vegetation-C enhancement by nitrogen deposition ~~reduces at the end of the 21^{st} century compared to values simulated during the middle of~~

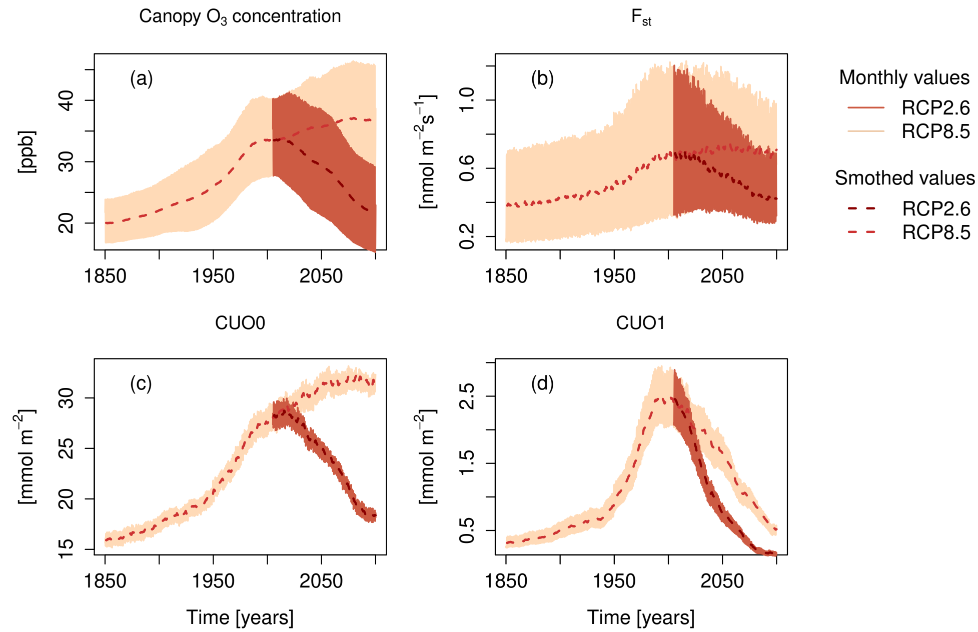

Figure 3. Simulated canopy O_3 concentration, ~~ozone~~ O_3 uptake (F_{st}), cumulative O_3 uptake without a flux threshold (CUO0) and cumulative O_3 uptake above a flux threshold of 1 $\mathrm{nmol\,m^{-2}\,s^{-1}}$ (CUO1) of the factorial run S5 (all forcing variables are simulated transient). Displayed are monthly values ~~(solid lines)~~ and smothed values ~~(broken line)~~ where the effect of the seasonal cycle is smoothed by the application of a moving average of 12 month.~~Brown lines: RCP2.6, red lines: RCP8.5~~

~~the~~ peaks around the mid 21^{st} century and declines thereafter. The soil-C is less affected by nitrogen deposition and maximal increases of ≈ 1 % (6 PgC) compared to pre-industrial values are simulated at the end of the 21^{st} century. Nitrogen deposition ~~stimulates~~ enhances the simulated land carbon sink (land C flux) ~~the strongest~~ most in the period between 1950 and 2050 by 5–25 % (-0.02~~–~~ ... -0.15 $\mathrm{PgC\,yr^{-1}}$) compared to pre-industrial values.

Nitrogen deposition steadily increases plant nitrogen uptake until the middle of the 21^{st} century, with maximum simulated increases of about 40 $\mathrm{TgNH_4yr^{-1}}$ or 9 % (see Fig. 6 and ~~Appendix~~ Supplement Fig. S4). Concurrently, N deposition increases N_2O emissions by 0.7 $\mathrm{TgN_2Oyr^{-1}}$ (20 %) and NH_4 leaching of 10 $\mathrm{TgNH_4yr^{-1}}$ (100 %) compared to pre-industrial values are simulated. NO_3 leaching increases until the end of the 20^{th} century by 6 $\mathrm{TgNO_3yr^{-1}}$ (80 %) compared to pre-industrial values and declines again ~~thereafter~~afterwards.

3.3 Magnitude of ~~ozone~~ O_3 deposition impact

3.3.1 Ozone uptake

Projections of ~~ozone~~ O_3 uptake and damage are primarily controlled by the scenarios of ~~tropospheric~~ near surface O_3 (Fig. 4a,b). ~~However, foliar ozone uptake is reduced by increasing atmospheric concentrations because of its effect on the relationship~~

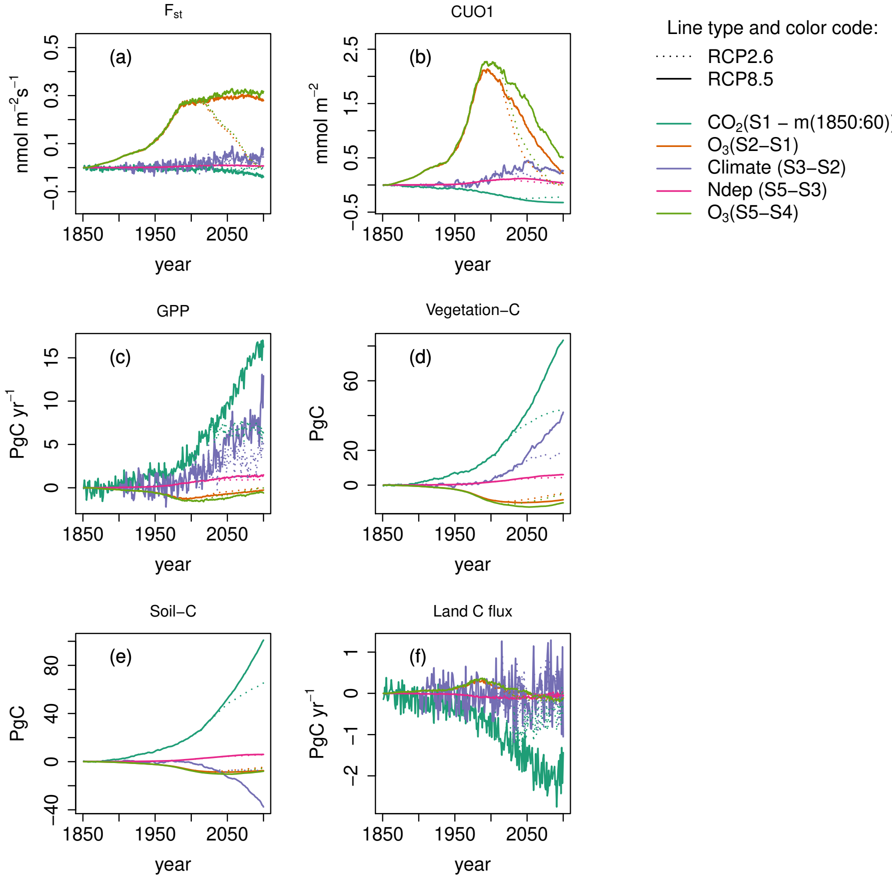

Figure 4. Single drivers obtained by subtracting factorial runs for selected output variables. Displayed are the results for simulated regional mean ~~ozone~~ O_3 uptake (F_{st}), regional mean cumulative canopy O_3 uptake above a flux threshold of $1\ \mathrm{nmol\,m^{-2}\,s^{-1}}$ (CUO1), regional summed GPP, regional summed stocks of total carbon biomass (vegetation-C), soil organic matter carbon (soil-C), and summed land carbon flux (land C flux) for simulations based on RCP2.6 and RCP8.5. The effect of the seasonal cycle is smoothed by the application of a moving average of 12 months(a,b).

~~between stomatal conductance and net photosynthesis. The effect of can also be seen in reduction of CUO1 during the 21^{st} century shown in Fig. 3. Lower stomatal conductances reduce F_{st} and CUO1, even if the concentrations slightly increase in simulations based on RCP8.5.~~

~~Nitrogen deposition slightly increases F_{st} by maximal 0.008 and 0.01 for RCP2.6 and RCP8.5, respectively (see Fig. 5a). This relates to an increase in CUO1 of about 1 %. Climate change increases stomatal ozone uptake about 0.04 during the 21^{st} century and considerably stronger compared to -deposition.~~

The simulated mean ~~ozone~~ O_3 uptake (F_{st}) due to changes in near surface O_3 concentration increases by approximately $0.27\ \mathrm{nmol\,m^{-2}\,s^{-1}}$ (70 %) between the pre-industrial period and the year 2000 (see Fig. 7a). Under the RCP8.5 scenario, F_{st}

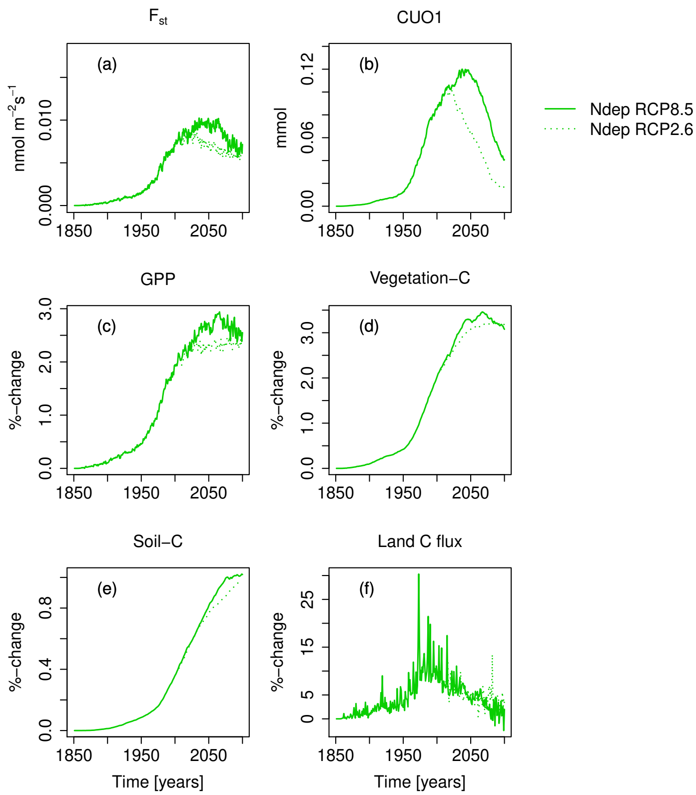

Figure 5. Nitrogen deposition induced absolute change in regional mean ~~ozone~~ O_3 uptake (F_{st}), mean cumulative O_3 uptake above a flux threshold of 1 $\mathrm{nmol\,m^{-2}\,s^{-1}}$ (CUO1), and change in % ~~change~~ in summed GPP, summed carbon biomass (vegetation-C), summed carbon soil organic matter (soil-C), and summed land carbon flux (land C flux) compared to pre-industrial values in the simulation region. The nitrogen deposition induced change is calculated from the simulation runs S3 and S5 (see Tab. 2). Solid lines indicate results from simulations based on RCP8.5, dotted lines results from simulations based on RCP2.6. The effect of the seasonal cycle is smoothed by the application of a moving average of 12 months (a,b).

increases until the end of the 21^{st} century, reaching more than a 90 % increase compared pre-industrial times. Conversely, in simulations based on RCP2.6, F_{st} declines strongly and by the end of the 21^{st} century comparable values to simulations based on pre-industrial O_3 concentrations are reached. The mean CUO1 increases by approximately 2.3 $\mathrm{mmol\,O_3\,m^{-2}}$ until the year 2000 and strongly declines until the end of the 21^{st} century (see Fig. 7b). In simulations based on RCP2.6 the CUO1 values reach comparable values to simulations based on pre-industrial O_3 concentrations by 2099.

However, foliar O_3 uptake is reduced by increasing atmospheric CO_2 concentrations because of its effect on the relationship between stomatal conductance and net photosynthesis. The effect of CO_2 can also be seen in reduction of CUO1 during the 21^{st} century shown in Fig. 3. Lower stomatal conductances reduce F_{st} and CUO1, even if the O_3 concentrations slightly increase in simulations based on RCP8.5. Nitrogen deposition slightly increases F_{st} by at most 0.008 $\mathrm{nmol\,m^{-2}\,s^{-1}}$ and

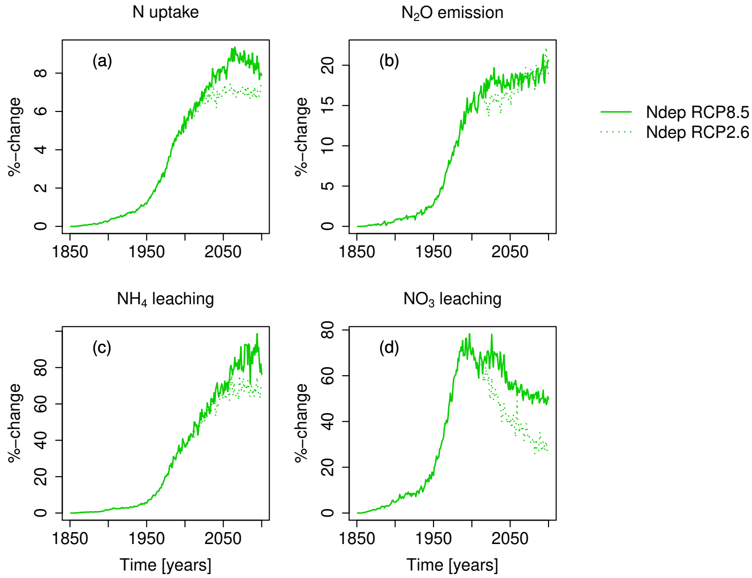

Figure 6. Nitrogen deposition induced change in % ~~change~~ in ~~regional summed~~ total N uptake by region, N_2O emission, NH_4 leaching and ~~N_2O~~ NO_3 leaching compared to pre-industrial values in the simulation region. The nitrogen deposition induced change in % ~~change~~ is calculated from the simulation runs S3 and S5 (see Tab. 2). Solid lines indicate results from simulations based on RCP8.5, dotted lines results from simulations based on RCP2.6.

0.01 $\mathrm{nmol\,m^{-2}\,s^{-1}}$ for RCP2.6 and RCP8.5, respectively (see Fig. 5a). This relates to an increase in CUO1 of about 1 %. Climate change increases stomatal O_3 uptake about 0.04 $\mathrm{nmol\,m^{-2}\,s^{-1}}$ during the 21st century and considerably stronger compared to N-deposition.

The two different approaches to assess the contribution of O_3 to the simulated trends in the carbon cycle based on analysing alternative combinations of model drivers (see Tab. 2) yield similar but not identical results (see Fig. 7). Typically, the differences between the two approaches do not exceed 1 % except for CUO1, where larger relative changes occur for small absolute changes (see Fig. 7b).

3.3.2 Ozone damage

In the period of ~~1970-1990~~1970–1990, i.e. the time of the peak increase on ~~tropospheric ozone~~ near surface O_3 concentrations, the simulated detrimental effects of O_3 on ~~photosynthesis~~ GPP nearly completely counteract the positive effect of rising CO_2 concentrations (see Fig. 4c). The negative impact of O_3 on GPP shows a maximum approximately in the 1990s at approximately -1.5 $\mathrm{PgC\,yr^{-1}}$ (4 %) compared to pre-industrial values (see Fig. 7c, ~~Appendix~~ Supplement Fig. S5 and Tab. 4). In the subsequent decades, the simulated ~~ozone~~ O_3 induced reduction in GPP declines to 1 % by the end of the 21st century for RCP8.5 and to close to zero for RCP2.6.

~~During the period 2000 to 2030, increasing dominates the change in GPP. After that time, GPP stagnates at 2030 levels due~~ Due to the stabilisation of atmospheric CO_2 in ~~RCP 2.6~~the RCP2.6 scenario, the increase in GPP levels off at 2040s levels, but continues to rise under RCP 8.5 with increasing CO_2. The growth-stimulating effect of N-deposition is smaller than the negative impact induced by O_3 during the 20^{th} century (see Fig. 4c). This pattern is reversed during the course of the 21^{st} century (see Section 3.4).

The O_3 effect on GPP propagates to vegetation and thus considerably affects the simulated ~~above- and below-ground biomass~~ total carbon biomass in vegetation (vegetation-C), and to a limited ~~extend~~ extent also soil-C storage. In the simulations with transient O_3 (S2,S3,S5), the regionally integrated ~~vegetation-C~~ vegetation-C ceases to grow in the 1950s for ~~30-50~~ 30–50 years (see in Fig. 2b), causing a loss of carbon storage compared to the simulations without increasing O_3 of about 8 Pg C (8 %). Despite the declining effect of O_3 on GPP, ~~vegetation-C~~ vegetation-C remains reduced for much of the first half of the 21^{st} century and only recovers very slowly ~~thereafter~~ afterwards (see Fig. 4c and d). The strongest ~~ozone~~ O_3 induced reduction in mean simulated vegetation-C in the simulation area occurs in the period of ~~2000-2020~~ 2000–2020 at approximately 10 % (see Fig. 7d and ~~Appendix~~ Supplement Fig. S5). The ~~ozone~~ O_3 effect on vegetation-C declines to 5 % by 2099 for RCP8.5 and 4 % for RCP2.6 (see Tab. 4). The soil-C is less strongly impacted by O_3 with simulated maximal reductions of less than 2 % (10 Pgc).

O_3 impact on land C storage (land C flux) peaks at the end of the 20^{th} century. In the 1990s, the effect of O_3 on the land sink is about 0.4 Pg C yr^{-1} or approx. 20 %. During the 21^{st} century, the ~~ozone~~ O_3 effect on the land C flux is reversed and eventually becomes positive. In the 2090s, the simulated land C flux is increased by about 4 to 7 % for RCP8.5 and 16 % for RCP2.6. This seemingly counter-intuitive effect is the result of lower ~~ozone-induced~~ O_3-induced net primary production, which reduces the formation of soil carbon. The resulting lower stock in soil carbon in simulations accounting for ~~ozone~~ O_3 damage results in lower increases in heterotrophic respiration due to climate change during the 21^{st} century, which causes the reversal of the O_3 effect on the land C sink.

3.3.3 Regional patterns

The simulated cumulative O_3 uptake above a flux threshold of 1 $\mathrm{nmol\,m^{-2}\,s^{-1}}$ (CUO1) shows a strong geographic variation. Highest values of CUO1 are simulated during the 1990s in the eastern and north-eastern US, large parts of ~~Europe central~~Central Europe, and eastern Asia (see ~~Appendix~~ Supplement Fig. S6a). Evergreen trees accumulate O_3 damage over several years, because of the longer life time of their leaves compared to deciduous trees. This can result in high values of CUO1, even if O_3 concentrations are moderate. At the end of the 21^{st} century simulated CUO1 values reach comparable values to pre-industrial times in large parts of the simulation region and slightly lower values in large parts of the US and Eurasia in simulations based on RCP2.6.

The highest ~~ozone~~ O_3 induced absolute reductions in GPP occur in Europe, Eastern US and Eastern Asia where the respective increase in CUO1 is highest. ~~Peak~~ During the 1990s, peak reductions of about ~~150-220~~ 150–220 $\mathrm{gCm^2yr^{-1}}$ (~~8-11~~ 8–11 %) are simulated in the eastern US, southern Europe and eastern Asia ~~during the decade of 1990~~ (see Fig. 8). Simulated ~~ozone induced damage to GPP declines~~ O_3 induced reductions in GPP decline in the decades of 2040 and 2090 for both RCPs ~~,~~

Table 3. Absolute and relative change in GPP, total carbon biomass in vegetation (vegetation-C), soil organic matter carbon (soil-C) and land carbon flux (land C flux) in deposition (Ndep), and O_3 concentrations. The differences in GPP, vegetation-C, soil-C and Land C flux are presented for simulations of the past years of 1850 to 2005 ~~, s~~ ~~2099,~~ and for the entire simulation period 1850 to 2099. The reported change refers to the change between the last and the first year of the respective time periods. The giver the O_3 impact.

RCP and time span	CO_2	CO_2	Climat
GPP	[$PgC\,yr^{-1}$]	[%]	[PgC yr
Past 1850:2005	3.4	11.5	3.1
RCP2.6 1850:2099	6.3	21.5	5.2
RCP8.5 1850:2099	16.3	55.6	12.9
~~RCP2.6 2006:2099 2.4 7.3 3 7.8 0.3 0.4 1.2...1.5 3.6...4.2 RCP8.5 2006:2099 12.4 37.4 12.9 28.4 0.8 0.5 0.9 2.8...3.2~~ vegetation-C	[PgC]	[%]	[PgC]
Past 1850:2005	18.3	23	4.9
RCP2.6 1850:2099	42.7	53.7	20.2
RCP8.5 1850:2099	83.8	105.4	41.9
~~RCP2.6 2006:2099 24.6 25.2 14.9 11.2 2.3 1 4.4...5 5.5...6.1 RCP8.5 2006:2099 65 66.1 37.5 22.1 4 0.8 0.1...0.6 4...4.9~~ soil-C	[PgC]	[%]	[PgC]
Past 1850:2005	23.2	4.4	-2.2
RCP2.6 1850:2099	64.8	12.2	-8.4
RCP8.5 1850:2099	100.5	18.9	-37.6
~~RCP2.6 2006:2099 41.7 7.5 -6.3 -1 3.4 0.6 2.6...2.8 0.5...0.6 RCP8.5 2006:2099 76.9 13.8 -35.5 -5.6 3.6 0.1...0.6 0.3 0.2~~ Land C flux	[$PgC\,yr^{-1}$]	[%]	[PgC yr
Past 1850:2005	-0.5	72.9	-0.4
RCP2.6 1850:2099	0.3	-39.1	-1
RCP8.5 1850:2099	-1.3	201.9	-1.1
~~RCP2.6 2006:2099 1.2 -76 -1.3 205.7 0.1 -5.1 -0.3...-0.4 29.4...45.5RCP8.5 2006:2099 -0.5 30.8 -1.9 116 0 -12.8 -0.2...-0.3 15.2...32.6~~			

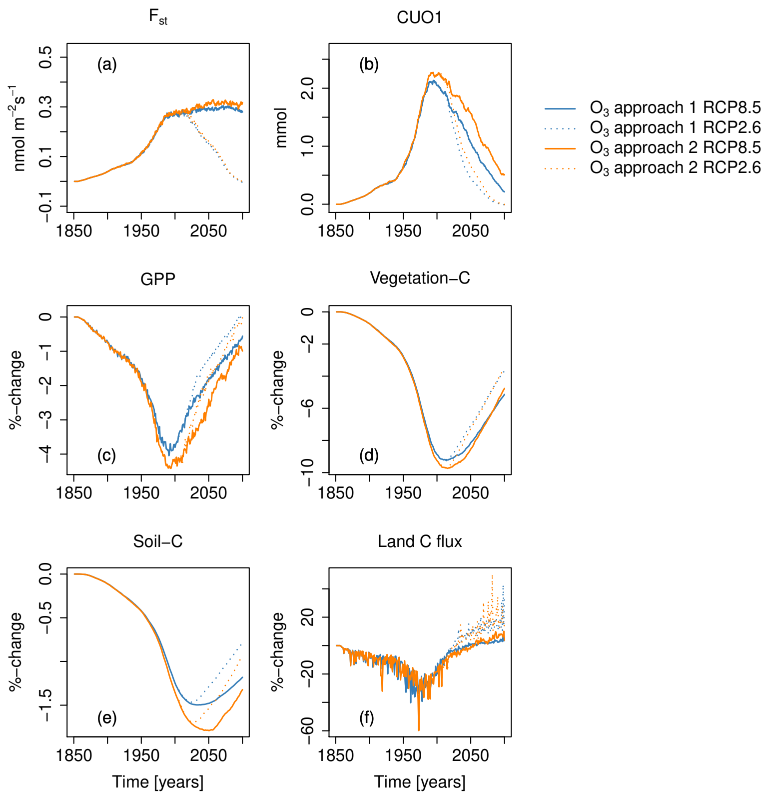

Figure 7. Ozone induced absolute change in regional mean ~~ozone~~ O_3 uptake (F_{st}), mean cumulative O_3 uptake above a flux threshold of $1\ \mathrm{nmol\,m^{-2}\,s^{-1}}$ (CUO1) and change in % ~~-change~~ in summed GPP, ~~summed~~ total carbon biomass in vegetation (vegetation-C), summed carbon soil organic matter (soil-C), and summed land carbon flux (land C flux) compared to pre-industrial values in the simulation region. Different colors indicate different approaches to calculate the ~~ozone~~ O_3 induced change from the factorial runs. Orange lines represent approach 1: (S2-S1)/S1, blue lines approach 2:(S5-S4)/S4. Solid lines indicate results from simulations based on RCP8.5, dotted lines results from simulations based on RCP2.6. The effect of the seasonal cycle is smoothed by the application of a moving average of 12 months.

~~but considerable ozone~~ and in many regions, while considerable O_3 induced reductions in GPP are simulated until the end of the 21st century in eastern Asia. In the ~~decade of 2040~~ 2040s under the RCP8.5 scenario relative reductions in GPP of ~~4-8~~ 4–8 % are simulated in southern Europe, parts of the eastern and western ~~US in simulations based on RCP8.5. Peak~~ USA, while peak relative decreases of ~~8-11~~ 8 – 11 % are simulated in eastern Asia. ~~At~~ Towards the end of the 21st century ~~ozone~~ O_3 induced reductions in GPP continue to decline, but reductions of above 8 % are still simulated in small parts of eastern Asia. Slight increases in GPP are simulated in a large fraction of the Eastern US and small scattered areas in Asia. Simulations based on RCP2.6 indicate for the end of the 21st century close to no ~~ozone~~ O_3 induced damage compared to pre-industrial values over large parts of the simulation ~~scope~~domain. Small absolute reductions are simulated in parts of Europe and small absolute increases are simulated in the Eastern US induced by lower CUO1 values compared to pre-industrial values (see ~~Appendix~~ Supplement Fig. S6). Increased atmospheric CO_2 concentrations compared to pre-industrial values reduce the stomatal conductance, restrict ~~ozone~~ O_3 uptake and enable the increase in GPP values.

As expected, O_3 impacts on vegetation-C and soil-C peak later compared to GPP (see Fig. 7c-e and Tab. 4). For both scenarios, the strongest ~~ozone~~ O_3 induced absolute reductions in vegetation-C of ~~1400-1600~~ 1400–1600 gCm^2 occur in the decade of 2040 in the eastern US, southern Europe and eastern Asia (see Fig. 10). For both RCPs the ~~ozone~~ O_3 induced vegetation-C reductions exceed 20 % in parts of Europe, eastern and western US and eastern Asia in the middle of the 21^{st} century. By the end of the 21^{st} century the ~~ozone~~ O_3 induced vegetation-C reduction attenuates in these hotspots for both RCPs, though stronger in simulations based on RCP2.6.

~~Ozone impacts on vegetation-and soil-peak later compared to GPP (see Fig. 7c-e and Tab. 4).~~

Table 4. Mean percent change in GPP, total carbon biomass in vegetation (vegetation-C), and land carbon flux (land C flux) induced by ~~ozone~~ O_3 during the decades of 1990 (~~1990-1999~~1990–1999), 2040 (~~2040-2049~~2040–2049) and 2090 (~~2090-2099~~2090–2099) compared to pre-industrial values for the Northern Hemisphere north of 30°N (NH30), Europe, USA and China. The given range indicates the estimates according to both approaches to calculate the ~~ozone~~ O_3 impact. The spread in the effect sizes due to inter-annual variability, derived from error propagation of the yearly estimates is displayed in Supplement Tab. S1.

Region	Pollutant	1990	2040 RCP8.5	2040 RCP2.6	2090 RCP8.5	2090 RCP2.6
GPP						
NH30	O_3	-3.8...-4.3	-2.0...-2.8	-1.3...-2.0	-0.7...-1.0	0...-0.2
NH30	Ndep	1.8	2.7	2.3	2.5	2.4
Europe	O_3	-4.5...-4.9	-2.2...-2.6	-1.4...-1.9	-0.8	-0.2...-0.3
Europe	Ndep	2.7	3.8	2.9	2.9	2.5
USA	O_3	-4.7...-5.0	-2.1...-2.7	-1.7...-2.1	-0.8...-1.1	0.3...1.0
USA	Ndep	1.4	1.1	0.9	0.6	0.9
China	O_3	-9.2...-10.1	-7.8...-10.8	-7.1...-8.6	-1.6...-2.8	-3.8...-5.7
China	Ndep	2.9	5.5	6.1	6.4	7
~~vegetation-~~Vegetation-C						
NH30	O_3	-8.5...-8.9	-8.4...-8.8	-7.4...-7.6	-5.1...-5.4	-3.8...-3.9
NH30	Ndep	1.8	3.3	3	3.2	3.2
Europe	O_3	-10.8...-11.5	-9.9...-10.6	-8.8...-9.3	-6.1...-6.4	-4.9
Europe	Ndep	3.2	4.7	4.2	3.6	4
USA	O_3	-11.9...-12.5	-10.8...-11.7	-9.7...-10.2...	-6.5...-6.8	-4.1...-4.3
USA	Ndep	1.6	1.8	1.7	1.5	1.3
China	O_3	-15.1...-15.9	-26.3...-29.3	-22.9...-24.4	-15.8...-18.5	-16.2...-16.4
China	Ndep	1.6	2.8	4	3.9	6.2
~~Land C~~Land C flux						
NH30	O_3	-20.7...-21.2	0...-2.2	6.2...7.4	3.5...6.9	15.7...16.2
NH30	Ndep	9.7	5	4.9	1.6	3
Europe	O_3	-23.7...-25.6	0.4...-1.7	9...9.9	4.6...15.7	15...17.1
Europe	Ndep	15.6	5.9	4.4	-6.7	-0.2
USA	O_3	-18.4...-20.4	0.6...1.1	8.3...10.1	2.9...6.4	16.4...19.9
USA	Ndep	4.3	0.7	-0.7	-1.9	0.9
China	O_3	-58.8...-62.9	-7.3...-12.8	-1.1...-1.7	11.3...24.8	24.9...30.7
China	Ndep	24.6	9.9	13.8	14.1	15.4

3.4 Comparative impact of N deposition and O_3

The magnitude of ~~ozone~~ the O_3 induced damage on GPP exceeded the growth stimulating effect induced by nitrogen deposition over large parts of the 20th century and until the beginning of the 21^{st} century (see Fig. 4c). ~~Contrary to the tropospheric~~ In contrast to the near surface O_3 concentrations, the regional mean nitrogen deposition does not decline during the 21^{st} century but slightly increases in RCP8.5 and RCP2.6. The growth stimulating effect on GPP induced by nitrogen deposition becomes higher in magnitude during the 21^{st} century compared to the detrimental effect of ~~ozone~~ O_3 (see Fig. 4c, Supplement Fig. S8 and Tabs. 4 and ~~??~~4).

The growth stimulating effect of nitrogen deposition on vegetation-C remains lower in magnitude compared to the detrimental effects of ~~ozone for both pollution~~ O_3 for both emission scenarios throughout the entire simulation period (see Fig. 4d and Tab. 3). However, in simulations based on RCP2.6 the ~~ozone~~ O_3 induced reduction on vegetation-C is at the end of the 21^{st} century only slightly higher in magnitude compared to the growth stimulating effect induced by nitrogen deposition (see Tabs. 4~~and ??~~).

The ~~extend~~ extent of simulated impact of ~~ozone~~ O_3 and nitrogen deposition on the terrestrial carbon uptake (GPP) and storage (vegetation-C) differs strongly within the simulated region. Nitrogen deposition stimulates GPP compared to simulations run with pre-industrial deposition values mainly in Europe and Eastern Asia. Simulated increases of GPP in these regions constitute about ~~80-140~~ 80–140 $\mathrm{gC\,m^2\,yr^{-1}}$ for simulations run based on RCP8.5 (see left column in Fig. 8). In relative terms, peak increases of ~~10-16~~ 10–16 % are found in parts of eastern, central and northern Asia and small parts of Europe (see ~~Appendix~~ Supplement Fig. S7). Simulated increases in GPP are higher, and hotspot areas more extended, in the decade of 2090 compared to the 2040 decade for both RCPs (see Supplement Fig. S8). Simulations based on RCP2.6 exhibit similar patterns compared to simulations based on RCP8.5, but show a less strong increase in GPP induced by to nitrogen deposition.

Nitrogen deposition induces peak increases in vegetation-C of ~~500-600~~ 500–600 $\mathrm{gC\,m^2}$ compared to pre-industrial values in parts of Europe and eastern Asia (see Fig. 10). Highest relative increases in vegetation-C of ~~14-17~~ 14–17 % are simulated in the decades of 2040 and 2090 in regions of southern and northern Asia, where absolute changes are mostly small.

~~Mean percent change in GPP, vegetation-, and land carbon flux (land flux) induced by nitrogen deposition during the decades of 1990 (1990-1999), 2040 (2040-2049) and 2090 (2090-2099) compared to pre-industrial values for the Northern Hemisphere north of 30°N (), Europe, USA and China. Region 1990 2040 RCP8.5 2040 RCP2.6 2090 RCP8.5 2090 RCP2.6 GPP 1.8 2.7 2.3 2.5 2.4 Europe 2.7 3.8 2.9 2.9 2.5 USA 1.4 1.1 0.9 0.6 0.9 China 2.9 5.5 6.1 6.4 7~~

~~vegetation-1.8 3.3 3 3.2 3.2 Europe 3.2 4.7 4.2 3.6 4 USA 1.6 1.8 1.7 1.5 1.3 China 1.6 2.8 4 3.9 6.2~~

~~Land Cflux 9.7 5 4.9 1.6 3Europe 15.6 5.9 4.4 -6.7 -0.2 USA 4.3 0.7 -0.7 -1.9 0.9 China 24.6 9.9 13.8 14.1 15.4~~

3.5 Impact of the ~~ozone~~ O_3 deposition scheme

~~Simulations run with a model version where the ozone deposition scheme is turned offresult in considerably higher estimates of F_{st} and CUO1, leading to higher damage estimates (see Fig. 9). In these simulations~~ In the simulations presented in the previous sections, O-CN was applied with its O_3 deposition scheme turned on. To test the impact of the application of the

O_3 deposition scheme on the estimated ozone damage, we reran the simulations with the O_3 deposition scheme turned off. In simulations where the O_3 deposition scheme is turned off the O_3 is assumed to enter leaves directly without accounting for the turbulent transport ~~in~~ between the lower troposphere and the leaves, as well as the deposition and destruction of ~~ozone~~ O_3 on other surfaces. Turning off the O_3 deposition scheme result in considerably higher estimates of F_{st} and CUO1, resulting in higher damage estimates (see Fig. 9). In simulations where the ~~ozone~~ O_3 deposition scheme is turned off, ~~ozone-induced~~ O_3-induced reductions in GPP and vegetation-C are approximately twice as high compared to simulations where the ~~ozone~~ O_3 deposition scheme is turned on. Peak reductions of GPP amount 3 $\mathrm{PgC\,yr^{-1}}$ (≈8 %) compared to approximately 1.5 $\mathrm{PgC\,yr^{-1}}$ (≈4 %) in simulations where the deposition scheme is turned on. At the end of the 21^{st} century the simulated reductions in vegetation carbon storage (vegetation-C) constitute 25 PgC (≈11 %) in simulations where the deposition scheme is turned off and 10 PgC (≈5 %) in simulations where the deposition scheme is turned driven by the RCP8.5 scenario. As for GPP and vegetation-C, the omission of the ~~ozone~~ O_3 deposition scheme causes roughly a doubling of the simulated damage to carbon soil organic matter (soil-C) and summed land carbon flux (land C flux).

4 Discussion

The simulations of the Northern Hemisphere biosphere from ~~1850-2099~~ 1850–2099 according to the representative concentration pathway scenarios ~~RCP8.5 and RCP2.6~~ 2.6 and 8.5 indicate that air pollution (~~ozone~~ O_3 and nitrogen deposition) may have considerably affected carbon uptake and plant growth in the past and ~~has the potential to~~ will continue to have a considerable impact during the 21^{st} century. ~~We simulate an ozone~~

In our simulations, nitrogen deposition stimulates the simulated land carbon sink of the Northern Hemisphere ≥ 30°N the strongest in the period between 1950 and 2050 by 5–25 % (0.02... 0.15 $\mathrm{PgC\,yr^{-1}}$) compared to pre-industrial values.

These values are broadly consistent with a meta-analysis by Schulte-Uebbing and de Vries (2018), who estimated that nitrogen stimulates the global land carbon sink in above ground and below ground woody biomass by 0.112–0.243 $\mathrm{PgCyr^{-1}}$. Global carbon storage in forests was estimated to increase about 0.27 $\mathrm{PgCyr^{-1}}$ induced by N deposition for the period 1997—2013 in simulations based on RCP4.5 (Wang et al., 2017). Thomas et al. (2010) found that above-ground biomass increment increased by 40 % compared to pre-industrial conditions in the northeastern and north-central USA during the 1980s and 1990s, from which they estimate that N deposition stimulates global tree carbon storage by 0.3 $\mathrm{PgCyr^{-1}}$.

Our simulations indicate an O_3 induced reduction in the land C flux of 0.4 $\mathrm{PgCyr^{-1}}$ in the ~~1990s.~~ decade of 1990. During the 21^{st} century the ~~ozone~~ O_3 effect on the land C flux is reversed and becomes positive. This is caused by lower increases of soil respiration due to climate change as a result of ~~ozone-induced~~ O_3-induced declines of net primary production and thus litterfall. This highlights the importance of investigating interactive processes on longer time scales together to get a better understanding of their net effect on the land carbon sink.

The stimulating effect of nitrogen deposition on regional mean GPP and biomass is lower in magnitude compared to the detrimental effect of O_3 during most of the simulation period for both RCPs (results for RCP2.6 not shown). Both effects approximately even out in their impact on the mean regional GPP by 2030–2050. By the end of the 21^{st} century nitrogen deposition stronger increases GPP than O_3 impacts decline it. However, regions that experience strong ~~ozone~~ O_3 induced negative effects do not always coincide with regions that benefit from the stimulating effect of nitrogen deposition (see Supplement Fig. S8).

During the 21^{st} century the cumulative O_3 uptake above a flux threshold of $1\ \mathrm{nmol\,m^{-2}\,s^{-1}}$ (CUO1), on which the damage calculations base, declines due to the impact of the CO_2 fertilisation effect on stomatal conductance and ~~ozone~~ O_3 uptake. This result is in agreement with Oliver et al. (2018), who found in Europe-wide simulations that elevated future CO_2 levels and reductions in O_3 concentrations result in reduced O_3 induced damage values by 2050. Induced by the simulated decline in CUO1 the mean regional reduction in GPP ~~deceases~~ decreases in the decade of 2050 to approximately 2 % in simulations based on RCP8.5 and 1–1.5 % in simulations based on RCP2.6. By the end of the 21^{st} century damage induced by elevated levels of O_3 decreases to approximately 1 % in simulations based on RCP8.5 and close to zero for RCP2.6. Simulations with the JULES model estimate a 8–15 % reduction in global GPP between 1901–2100 (Sitch et al., 2007). A more recent version of the JULES model suggest a 4–9 % reduction in European GPP due to ~~ozone~~ O_3 between 1901 and 2050 (Oliver et al., 2018). Both estimates are higher compared to the simulation results here (see Tab. 4).

Our estimates of the impact of ~~ozone~~ O_3 on the land C sink is smaller than that by Oliver et al. (2018), who simulated an ~~ozone~~ O_3 induced reduction of the land C sink by -0.7~~–~~... -1.3 PgC in the decade of 1970. The simulated detrimental ~~ozone~~ O_3 effect declines in the following decades to -0.3~~–~~... -0.5 PgC in the period of 2002–2011. A possible reason for the higher estimates by Sitch et al. (2007) ~~and Oliver et al. (2018)~~ is the absence of an ~~ozone~~ O_3 deposition scheme in JULES, what might have caused higher surface ~~ozone~~ O_3 concentrations and hence increased ~~ozone~~ O_3 uptake and incurred damage. The ~~tropospheric~~ near surface O_3 concentrations used in the simulations here to force the model ~~are provided by CTMs which~~ report O_3 concentrations in a height of approximately 45 m above the surface. The ~~ozone~~ O_3 deposition scheme included into O-CN uses the O_3 concentration of the free ~~atmosphere~~ troposphere to calculate the O_3 concentration at canopy level.

If the O_3 concentration ~~provided by the CTMs~~ from the forcing is used as if being at canopy level the O-CN model simulates a higher ~~ozone~~ O_3 uptake. Following this twice as high damage values to GPP and vegetation-C are calculated compared to simulations where the deposition scheme is applied to calculate the canopy level O_3 concentration. This highlights the importance of using canopy level O_3 concentrations to calculate ~~ozone~~ O_3 uptake and damage to prevent a considerable overestimation of ~~ozone~~ O_3 induced damage.

4.1 Air pollution impacts on GPP and total carbon biomass

The average ~~ozone~~ O_3 effect on GPP in the Northern Hemisphere ($\geq 30°$N) increases until the ~~decade of 1990~~1990s, when GPP is reduced by approximately 4 % compared to the pre-industrial period. Regional hotspots in southern Europe, eastern Asia and the eastern US exhibit ~~ozone~~ O_3 induced reductions of 8–11 % for the decade of 1990. In a meta-analyses by Wittig et al. (2009) net photosynthesis damage of trees grown in ambient O_3 concentrations vs. charcoal filtered air is estimated to amount 11 % and 19 % for trees grown in elevated O_3 concentrations vs. charcoal filtered air. Lombardozzi et al. (2013) estimates damage to net photosynthesis of temperate deciduous trees to amount 12 % and 16 % for temperate evergreen trees. A reduction of 28 % in net photosynthesis is estimated for woody plants grown in elevated O_3 compared to a control by Li et al. (2017). Simulated ~~ozone~~ O_3 damage values in hotspot areas are close to the lower damage estimates suggested by Wittig et al. (2009) and Lombardozzi et al. (2013), while the regional means including many areas with low O_3 exposure, results in lower average ~~ozone~~ O_3 damage than estimated by these meta-analyses.

Several ~~process based models estimated ozone~~ process-based models estimated O_3 induced damage to ~~NPP/GPP~~ GPP or net primary production (NPP) on global or regional scale: a mean global ~~ozone~~ O_3 induced reduction in NPP of 0.8–2.9 % from 1989 to 1993 is estimated by the Terrestrial Ecosystem Model (Felzer et al., 2005). Simulations with the Community Land Model suggest a 10.8 % reduction of global mean GPP for present day O_3 concentrations (Lombardozzi et al., 2015). A mean reduction in NPP of 4.5 % in China between ~~1961-2000~~ 1961–2000 is estimated by a process-based Dynamic Land Ecosystem Model (Ren et al., 2007). The simulation of ~~ozone~~ O_3 damage to China's forests suggest a 0.2–1.6 % decrease in NPP from the 1960s to ~~2000 – 05~~ 2005 (Ren et al., 2011). Simulations using the Terrestrial Ecosystem Model estimate a mean reduction in NPP of 2.6–6.8 % in the United States for the period of the late 1980s to early 1990s (Felzer et al., 2004). The YIBS model simulates a 4–8 % damage to GPP due to O_3 in the eastern US and 8–17 % damage in hot spots for the decade of 1998–2007 (Yue and Unger, 2014). In the Euro-Mediterranean region a reduction in GPP of 22 % is estimated for the year 2002 by the ORCHIDEE model (Anav et al., 2011). The mean GPP of the years 2001–2010 in Europe is simulated to be reduced by 7.6 % compared to not accounting for ~~ozone~~ O_3 damage by the O-CN model (Franz et al., 2017). Here, on a regional mean basis ~~ozone~~ O_3 induced reductions of about 4 % are simulated at the end of the 20^{th} century and beginning of the 21^{st} century compared to pre-industrial values. At the end of the 21^{st} century close to zero ~~ozone~~ O_3 induced reductions in GPP are simulated by O-CN here. An exception are hot spots like Eastern Asia where peak decreases of more than 8 % are simulated for both RCPs at the end of 21^{st} century. Our damage estimates here are lower compared to at least most of the previous estimates suggested by biosphere models.

~~The ozone induced simulated mean~~ In our simulations, the O_3 induced regional reduction in total ~~above- and below-ground carbon biomass~~ carbon biomass in vegetation (vegetation-C) reaches peak values of 8–10 % at the end of the 20^{th} and first half of the 21^{st} century. Damage values of 20–23 % are simulated in damage hotspots in southern Europe, eastern Asia and the eastern and western US for the decade of 1990 (see ~~Appendix~~ Supplement Fig. S9). A meta-analyses conducted with trees suggests a 7 % reduction in total biomass for trees grown in ambient air compared to charcoal filtered air and a 17 % reduction for trees grown in elevated O_3 concentrations compared to charcoal filtered air (Wittig et al., 2009). In a meta-analyses by Li et al. (2017) a 14 % reduction in total biomass is calculated for trees grown in elevated O_3 concentrations (mean of 116 ppb) compared to controls grown in a mean O_3 concentration of 21 ppb. The simulated regional mean estimate of ~~ozone~~ O_3 induced damage to vegetation-C is higher compared to the estimate of trees grown in ambient vs. charcoal filtered air by Wittig et al. (2009) and lower compared to trees grown in elevated O_3 vs. charcoal filtered air or a mean of 21 ppb O_3 (Wittig et al., 2009; Li et al., 2017). Simulated damage values in the hotspots are higher compared to the estimates by the meta-analyses.

Our simulated declines in ~~ozone~~ O_3 induced damage to GPP and vegetation-C during the 21^{st} century generally agree with simulated reductions in potential threat to vegetation by Klingberg et al. (2014).

Klingberg et al. (2014) report that by 2050 the ~~ozone~~ O_3 exposure index AOT40 (Accumulated exposure Over a Threshold of 40 ppb O_3) is projected to decrease over wide areas of Europe below critical levels defined by the EU directive 2008/50/EC and the LRTAP convention in simulations of ~~a chemical transport model (CTM)~~ the chemistry transport model MATCH driven by the RCP4.5 emission scenario. ~~The~~ Their simulations suggest that the more physiological based ~~ozone~~ O_3 damage index POD1 (Phytotoxic Ozone Dose above a threshold of 1 $nmol\, m^{-2}\, s^{-1}$) ~~is projected to decline~~ declines as well, however to a lesser ~~extend~~ extent compared to the AOT40 index and not below critical levels defined for forest trees (Klingberg et al., 2014).

An ensemble of six global atmospheric chemistry transport models project improvements of the AOT40 index in the Northern Hemisphere by 2099 under the RCP2.6 and RCP4.5, while critical levels continue to be exceeded over many areas (Sicard et al., 2017). By 2099 the potential impact of O_3 on photosynthesis and carbon assimilation is projected to decline by 61 % under the RCP2.6 scenario, by 47 % under RCP4.5 and increase by 70 % under the RCP8.5 scenario compared to the early 2000s (Sicard et al., 2017).

4.2 Interactive effects of O_3 and CO_2

Elevated levels of CO_2 (eCO_2) have the potential to induce stomatal closure (Paoletti and Grulke, 2005) what might limit O_3 uptake and damage. Contradictory evidence exists showing that either eCO_2 ameliorated the negative effects of O_3 on plants (Barnes and Pfirrmann, 1992; Broadmeadow and Jackson, 2000; Isebrands et al., 2001; Riikonen et al., 2004) or that there was little interaction between both gases and the stimulating effect of eCO_2 on NPP persisted (Talhelm et al., 2014; Zak et al., 2011). Results from the Aspen FACE indicate that stomatal conductance and ~~ozone~~ O_3 uptake were not reduced by eCO_2 in their experiment (Uddling et al., 2010), and that ~~ozone~~ O_3 fumigation completely offset the growth enhancement observed in the eCO_2 treatment for ~~ozone~~ O_3 sensitive and tolerant clones (Karnosky et al., 2003).

Several studies find species specific positive or negative impacts of ~~+~~eCO_2 and elevated levels of O_3 (eO_3) on photosynthesis (Noormets et al., 2001), growth (Isebrands et al., 2001) and biomass (King et al., 2005). An amplification of the negative effects of O_3 under eCO_2 on leaf chlorophyll content, nitrogen content and electron transport capacity (J_{max}) was observed in ~~ozone~~ O_3 sensitive and tolerant aspen clones (Noormets et al., 2010). A possible reason for the amplification of ~~ozone~~ O_3 induced negative effects under eCO_2 is a possible down regulation or suppression of antioxidant production under eCO_2 and hence increased injury (Wustman et al., 2001; Karnosky et al., 2003). All in all, a clear picture of the joint effects of eCO_2+eO_3 on plants or plant groups is still lacking.

Terrestrial biosphere models often assume a tight coupling between net photosynthesis and stomatal conductance ~~what~~ which induces stomatal closure in case of simulated eCO_2 and restricts O_3 uptake and damage (Felzer et al., 2004, 2005; Sitch et al., 2007; Oliver et al., 2018; Yue and Unger, 2014). For example Sitch et al. (2007) simulated a 6–9 % reduction in O_3 induced damage to GPP due to elevated levels of CO_2 and a 5–10 % reduction in the ozone-related effect on land carbon storage between the years 1901 and ~~2100.~~ 2100 in a scenario with strongly rising atmospheric CO_2. Oliver et al. (2018) simulated a 1–2 % decrease in O_3 induced damage to GPP and land carbon storage caused by elevated levels of CO_2 between 1901 and 2050. The largest simulated impact of ~~ozone~~ O_3 on the land carbon sink occurred during the 20th century when the ~~atmospheric~~ tropospheric O_3 concentration rose quickly (Oliver et al., 2018). During the 21th century simulated O_3 concentrations changed less and the simulated elevated levels of CO_2 restricted ~~O_3~~ O_3 uptake and induced damage (Oliver et al., 2018). This agrees well with our findings here that ~~ozone~~ O_3 induced damage increases from pre-industrial times until the end of the 20th century (GPP) or beginning of the 21st century (vegetation-C) and afterwards decreases again (see Fig. 7).

However, the ~~very simplistic~~ simulation of reduced ~~ozone~~ O_3 uptake and incurred damage induced by eCO_2 does not mirror all the effects observed in field experiments (Wustman et al., 2001; Karnosky et al., 2003; Noormets et al., 2010). Similar to other terrestrial biosphere models, O-CN does not account for observed effects like an exacerbation of ~~ozone~~ O_3 induced damage due to eCO_2 (Wustman et al., 2001; Karnosky et al., 2003) or unaltered rates of stomatal conductance and O_3 uptake under eCO_2 (Uddling et al., 2010). Following this the presented low values of simulated future ~~ozone~~ O_3 damage represent a possible future scenario under the assumption that the large majority of plants react to the ~~the~~ combined exposure to elevated levels of CO_2 and O_3 by a reduced stomatal uptake of O_3 and reduced incurred damage.

4.3 Limitations of comparisons between publications

When interpreting the comparison of ~~the results here~~ our results and previously published simulation results one has to keep in mind that the different modelling ~~approaches usually~~ set-ups and approaches differ in several aspects that ~~might considerably impact~~ considerably affect the damage estimate. Models often apply different injury functions which relate ~~ozone~~ O_3 uptake to plant damage (Lombardozzi et al., 2012, 2015; Franz et al., 2017; Oliver et al., 2018). However, injury functions have the potential to induce considerable over- or underestimation of simulated biomass damage compared to measured damage values (Franz et al., 2018). Simulations ~~often~~ differ in the ~~simulated time period~~ time period covered, e.g. Sitch et al. (2007) (~~1901-2100~~1901–2100), Lombardozzi et al. (2015) 25 years with an average O_3 concentration of the years ~~2002-2009~~2002–2009, Franz et al. (2017) (~~1961-2011~~1961–2011), and Oliver et al. (2018) (~~1901-2050~~1901–2050). They ~~differ in~~ also differ in the forcing considered e.g. the representation of changing CO_2 concentrations, nitrogen deposition and land-cover/ land-use change. For instance, Sitch et al. (2007) simulate changing CO_2 concentrations, ~~Lombardozzi et al. (2015) do include neither~~while Lombardozzi et al. (2015) does not, Franz et al. (2017) account for changing CO_2 concentrations, nitrogen deposition but use static land-cover (kept fixed at 2005 levels), and Oliver et al. (2018) simulate changing CO_2 concentrations and a partly fixed land-cover, but no effect of N deposition. Furthermore damage estimates are calculated based on different ~~references~~reference periods and conditions. Damage might be given as the difference between a simulation accounting for O_3 damage compared to a reference simulation not accounting for ~~ozone~~ O_3 damage (Lombardozzi et al., 2015; Franz et al., 2017). Another approach is to report the damage simulated between a specific time period. Sitch et al. (2007) calculate ~~ozone~~ O_3 induced damage between ~~1901-2100~~ 1901–2100 and Oliver et al. (2018) between ~~1901-2001 and 2001-2050~~1901–2001 and 2001–2050.

Different modelling studies apply differing ~~pollution~~ emission scenarios, e.g. IPCC SRES (Sitch et al., 2007) and the RCP scenarios used here, ~~what~~ which might impact simulated ~~ozone~~ O_3 uptake and incurred damage. The application of the IPCC SRES scenarios~~(~~, which assume a large increase in O_3 precursor emissions~~) results in a simulated~~ , implies an increase in annual global mean surface O_3 concentrations by ~~4-6~~ 4–6 ppb (Wild et al., 2012). Contrary to this, the application of the RCP scenarios (Moss et al., 2010; van Vuuren et al., 2011) in 14 global chemistry transport models results in the projection of declining annual global mean surface O_3 concentrations of as much as 2 ppb by 2050 in most regions of the globe except South Asia where increases are simulated (Wild et al., 2012). Lower projected ozone-induced damage in our study compared to Sitch et al. (2007) is therefore also a consequence of the assumed scenario.

Turnock et al. (2020) found that the CMIP6 models overestimate observed surface O_3 concentrations by up to 16 ppb across most regions of the globe. This will likely lead to a general overestimation of simulated O_3 damage by terrestrial biosphere models. However, the ozone deposition scheme included into O-CN has the potential to ameliorate this observed discrepancy. The calculation of canopy level O_3 concentrations from the lowest level O_3 concentrations of the forcing data are lower and thus probably closer to the observations.

A further important difference between the published results is the time resolution of the ~~ozone~~ O_3 forcing applied in the simulations. Some studies used hourly ~~ozone~~ O_3 forcing (e.g. Lombardozzi et al. (2015), Franz et al. (2017), and Oliver et al. (2018)) and others are forced by monthly diurnal mean values (e.g. Sitch et al. (2007) and the simulations here). As the formation of ~~ozone~~ O_3 shows a pronounced diurnal cycle (Sanz et al., 2007), the use of monthly mean ~~ozone~~ O_3 concentrations probably impacts the simulated estimates of ~~ozone~~ O_3 uptake. However, to which ~~extend~~ extent the omission of a diurnal cycle impacts ~~ozone~~ O_3 uptake, accumulation and damage estimates is yet uncertain.

4.4 Limits to the parameterisation of ~~ozone~~ O_3 damage in O-CN

Plants can activate defence mechanism and physiological pathways to produce protective compounds like ascorbate and polyamines which can detoxify at least part of the ozone taken up (Kangasjärvi et al., 1994; Kronfuß et al., 1998; Tausz et al., 2007). In the simulations conducted here we account for detoxification by introducing a flux threshold but do not account for the cost to produce protective compounds like antioxidants due to the lack of suitable data. This could potentially introduce a bias bias towards underestimating damage to GPP if the leaf-injury parameterisations are based on leaf-level data.

Ozone sensitivity is known to differ between plant groups, plant species and between genotypes (Wittig et al., 2007; Lombardozzi et al., 2013; Li et al., 2017; Hayes et al., 2007; Karnosky et al., 2003). The assumed injury function is a key aspect of the simulation of ~~ozone~~ O_3 damage and has a large impact on the ~~extend~~ extent of the estimated damage (Franz et al., 2018). However, the scarcity of suitable data restricts the possibility to parameterise injury functions for all simulated PFTs (e.g. 12 PFTs in O-CN), let alone a variation of the ~~ozone-sensitivity~~ O_3-sensitivity within PFTs. Furthermore it restricts the evaluation of ~~ozone-submodels~~ O_3-submodels and the included injury functions. The injury functions used for the simulations here are tuned to reproduce observed biomass damage from filtration/fumigation experiments of broadleaved and needle-leaved tree species (Franz et al., 2018). The simulations are restricted to the Northern Hemisphere $\geq 30°$N to limit the domain of simulation to temperate/boreal forests and thus similar species as used for the tuning of the injury functions. Due to the lack of suitable damage functions for grass species we here applied the damage functions developed to match damage to trees. This induces a bias in the damage estimates and will likely results in an underestimation of simulated damage for example for the crop plant functional types.

The biomass damage experiments used to parameterise the injury function ~~are~~ in O-CN were conducted with young trees grown in monocultures. The common attempt to estimate responses of adult trees grown under natural conditions by the extrapolation of results from short-term experiments with young trees is subject to several issues, e.g. due to the differing environmental conditions and changing ~~ozone~~ O_3 sensitivities with increasing tree size or age ~~(Schaub et al., 2005; Cailleret et al., 2018)~~

(Schaub et al., 2005; Cailleret et al., 2018; Franz et al., 2018). It is yet uncertain if the simulation of injury to photosynthesis based on experiments with young trees can be transferred to adult trees to obtain realistic biomass damage estimates.

Differing ~~ozone~~ O_3 sensitivities can induce changes in community composition (Barbo et al., 1998; Kubiske et al., 2007; Zak et al., 2011) as well as the interactive effects of changed CO_2 and O_3 concentrations (Karnosky et al., 2003). The responses of plants grown under interspecific competition, e.g. in forests, may not be transferred from results of filtration/fumigation experiments (with elevated CO_2 and/or O_3) of plants grown in monoculture (Kozovits et al., 2005). For instance, Zak et al. (2011) found that initial declines in forest productivity induced by elevated levels of O_3 were compensated for by the growth of ~~ozone~~ O_3 tolerant individuals resulting in an equivalent NPP between ambient and elevated levels of O_3. Simulations by an individual-based forest model indicate that O_3 damage might not reduce the carbon sequestration capacity ~~in forests might not be reduced by ozone damage if at the ecosystem level~~ of forests if the reduced carbon fixation of ~~ozone-sensitive~~ O_3-sensitive species is compensated ~~for by an~~ by increased carbon fixation of less ~~ozone-sensitive species~~ O_3-sensitive species at the ecosystem level (Wang et al., 2016). The simulation of community dynamics is limited in O-CN, as it does not account for species, and therefore acclimation processes at the ecosystem level are not accounted for. The effect of interspecific competition on ~~ozone~~ O_3 damage is not reflected in the used injury function as the experiments are conducted with monocultures. These two factors can contribute to an overestimation of simulated damage.

The application of present day land-use information fixed to the year 2000 in our simulations may affect simulated trends of GPP, canopy conductance and biomass production in regions where land cover and/or land-use have historically changed or are projected to change during the scenario period. This can lead to a discrepancy in the simulated effect of nitrogen deposition and O_3 damage. For example O_3 damage differs between plant functional types and a shift to highly productive crops would results in an increase in damage.

Holding the N fertiliser application at the year 2000 levels in our simulations here imposes a bias on the simulated GPP, biomass production and O_3 damage in regions where fertiliser application changed. Regions where fertiliser application decreased would show a reduction in growth stimulation along with a reduction in O_3 damage. Regions exposed to increases in fertiliser application would exhibit a stimulation in growth along with an increase in O_3 damage.

The simulations conducted here are run offline and following this atmosphere and biosphere do not feedback on one another. Forcing variables like O_3 concentrations and nitrogen deposition are provided by a different model than the climate. This imposes an inconsistency between the biosphere, climate and the abundance of the air pollutants whose formation depends on climate variables. This contributes to unavoidable inconsistencies between the atmospheric forcing and the land fluxes when making offline simulations compared to a simulation with a fully coupled Earth System Model. However, these limitations, do not invalidate the simulated sensitivity of the land carbon cycle simulation to the forcing applied.

5 Conclusion

O_3 damage considerably reduced simulated carbon uptake (GPP) and storage (vegetation-C) in the simulation area where the maximal impact occurs at the end of the 20^{th} century and beginning of the 21^{st} century respectively. The detrimental ~~ozone~~ O_3

impact declines during the 21^{st} century and reaches mean regional reductions of 0–1 % for GPP and 4–5 % for vegetation-C by the end of the 21^{st} century compared to pre-industrial values. However, in hotspots decreases in GPP of more than 8 % (eastern Asia) and decreases in vegetation-C of more than 15 % (parts of Europe, eastern and western US and eastern Asia) are simulated at the end of the 21^{st} century. Nitrogen deposition increases GPP less than O_3 impacts decrease it for most of the simulated period. The increasing effect of nitrogen deposition on vegetation-C is lower compared to the decreasing effect of O_3 for the entire simulation period. Accounting for the stimulating effects of nitrogen deposition but omitting the detrimental effect of O_3 can lead to an over estimation of carbon uptake and storage.

Acknowledgements. The research leading to this publication was supported by the EU Framework programme through grant no. 282910 (ECLAIRE) and the Max Planck Society for the Advancement of Science e.V. through the ENIGMA project. This project has received funding from the European Research Council (ERC) under the European Union's Horizon 2020 research and innovation programme (grant agreement no. 647204; QUINCY).

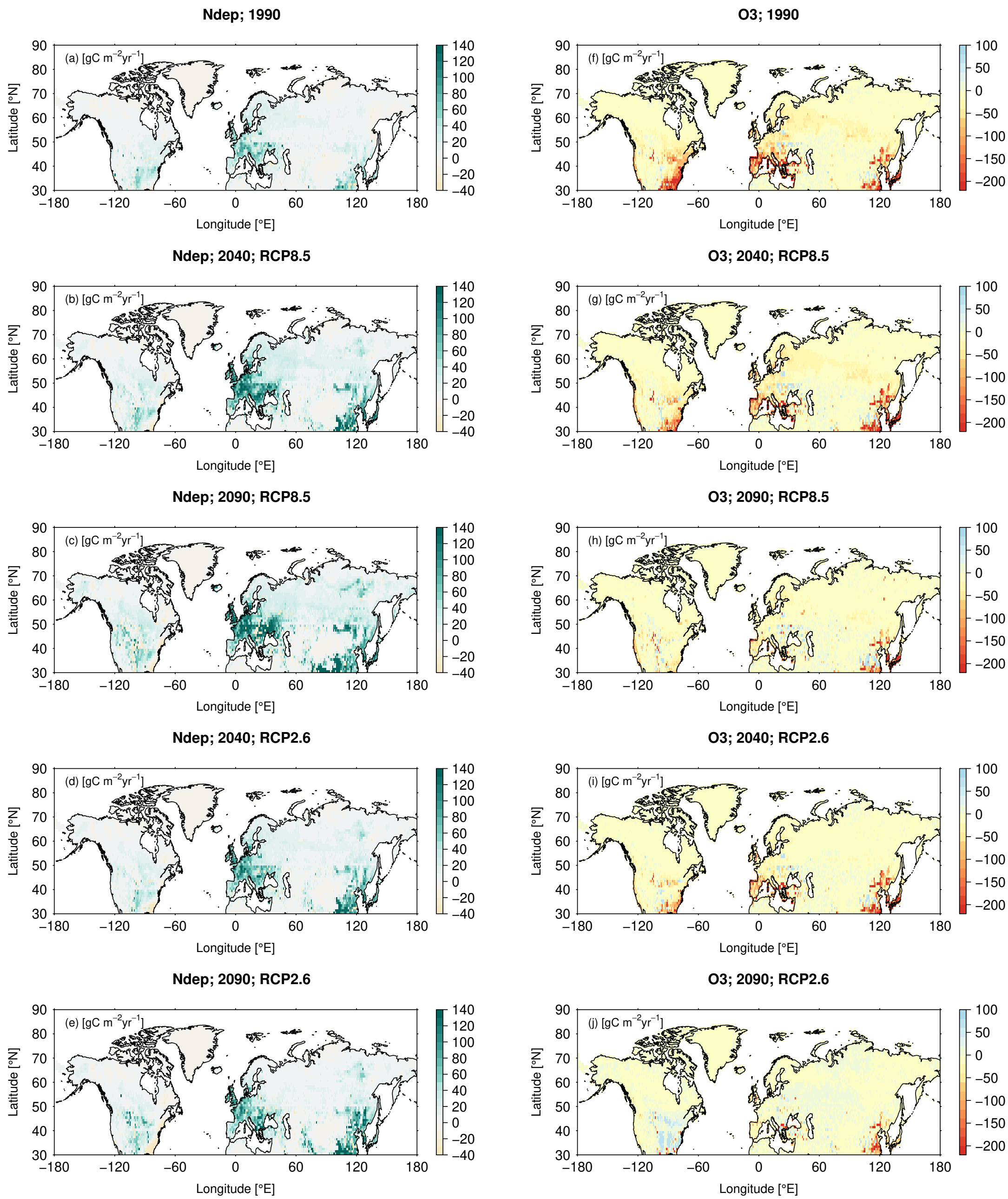

Figure 8. Absolute change in GPP compared to pre-industrial values induced by nitrogen deposition (left column) and ~~ozone~~ O_3 calculated according to approach 2 (right column). The induced change in GPP is displayed for the decades 1990 (mean of the years ~~1990-1999~~1990–1999), 2040 (mean of the years ~~2040-2049~~2040–2049) and 2090 (mean of the years ~~2090-2099~~2090–2099). For the decades 2040 and 2090 results from simulations based on RCP8.5 and RCP2.6 are displayed. See Tab. 2 for details on the calculation of the single drivers.

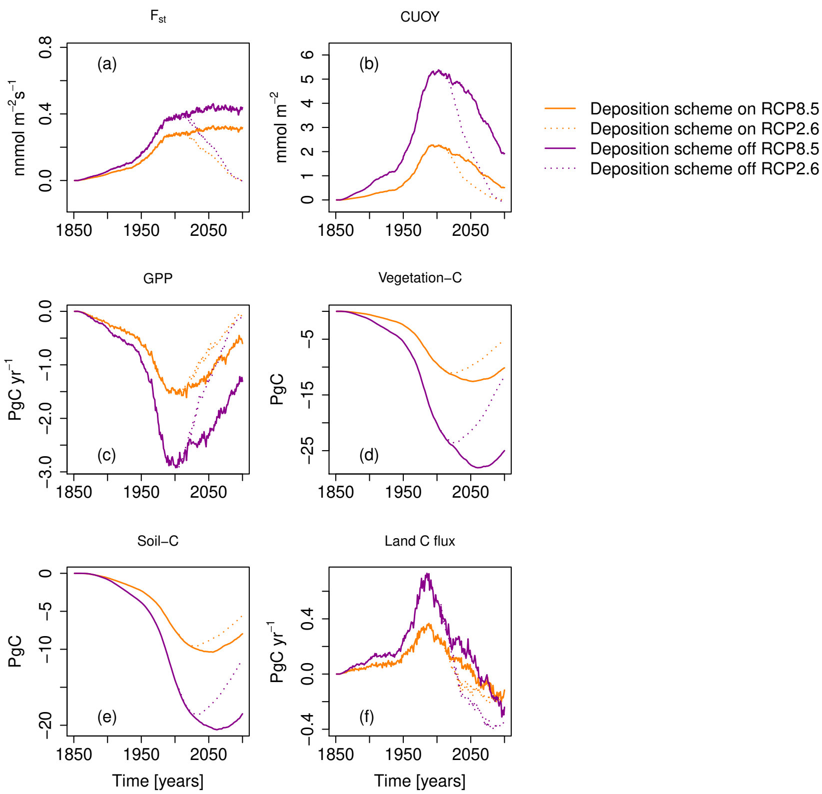

Figure 9. Ozone impacts on the regional mean ~~ozone~~ O_3 uptake (F_{st}), mean cumulative O_3 uptake above a flux threshold of $1\,\mathrm{nmol\,m^{-2}\,s^{-1}}$ (CUO1), summed GPP, ~~summed~~ total carbon biomass in vegetation (vegetation-C), summed carbon soil organic matter (soil-C), and summed land carbon flux (land C flux) compared to pre-industrial values in the simulation region. The displayed ~~ozone~~ O_3 impact is calculated based on approach 2. Orange lines: Results based on a model version where the ~~ozone~~ O_3 deposition scheme is turned on. Magenta lines: Results based on a model version where the ~~ozone~~ O_3 deposition scheme is turned off. Solid lines indicate results from simulations based on RCP8.5, dotted lines results from simulations based on RCP2.6. The effect of the seasonal cycle is smoothed by the application of a moving average of 12 months (a,b).

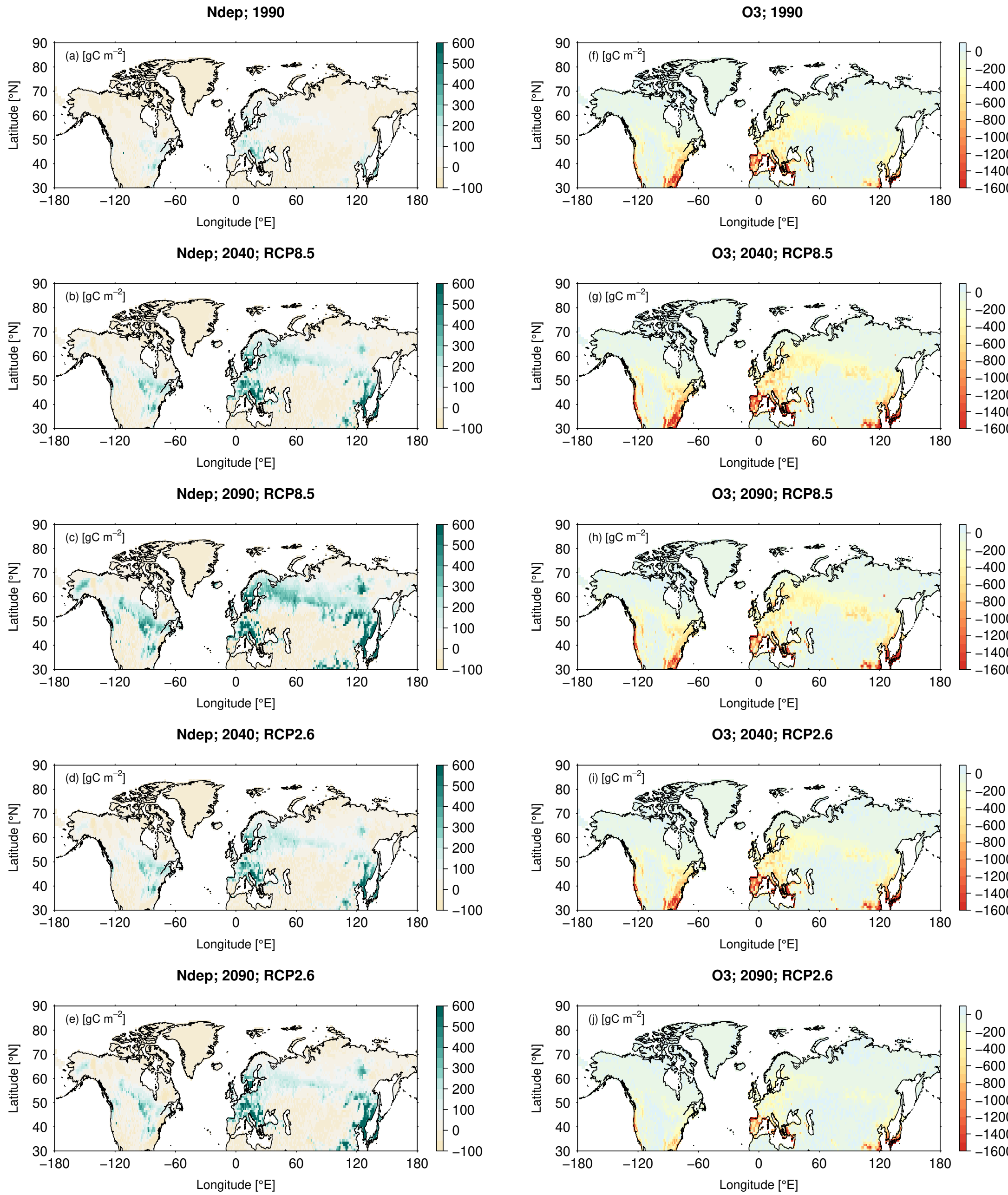

Figure 10. Absolute change in the total carbon biomass in vegetation (vegetation-C) compared to pre-industrial values induced by nitrogen deposition (left column) and ~~ozone~~ O_3 calculated according to approach 2 (right column). The induced change in the total carbon biomass is displayed for the decades 1990 (mean of the years ~~1990-1999~~1990–1999), 2040 (mean of the years ~~2040-2049~~2040–2049) and 2090 (mean of the years ~~2090-2099~~2090–2099). For the decades 2040 and 2090 results from simulations based on RCP8.5 and RCP2.6 are displayed. See Tab. 2 for details on the calculation of the single drivers.

References

Ainsworth, E. A. and Long, S. P.: What have we learned from 15 years of free-air CO_2 enrichment (FACE)? A meta-analytic review of the responses of photosynthesis, canopy properties and plant production to rising CO_2, New Phytologist, 165, 351–372, https://doi.org/10.1111/j.1469-8137.2004.01224.x, https://nph.onlinelibrary.wiley.com/doi/abs/10.1111/j.1469-8137.2004.01224.x, 2005.

Ainsworth, E. A., Yendrek, C. R., Sitch, S., Collins, W. J., and Emberson, L. D.: The Effects of Tropospheric Ozone on Net Primary Productivity and Implications for Climate Change, Annual Review of Plant Biology, 63, 637–661, 2012.

Akimoto, H.: Global Air Quality and Pollution, Science, 302, 1716–1719, 2003.

Anav, A., Menut, L., Khvorostyanov, D., and Viovy, N.: Impact of tropospheric ozone on the Euro-Mediterranean vegetation, Global Change Biology, 17, 2342–2359, 2011.

Ball, J., Woodrow, I., and Berry, J.: A Model Predicting Stomatal Conductance and its Contribution to the Control of Photosynthesis under Different Environmental Conditions, in: Prog. Photosynthesis Res. Proc. Int. Congress 7th, Providence. 10-15 Aug 1986, edited by Biggins, J., pp. 221–224, Progress in Photosynthesis Research, 1987.

Barbo, D., Chappelka, A., Somers, G., Miller-Goodman, M., and Stolte, K.: Diversity of an early successional plant community as influenced by ozone, The New Phytologist, 138, 653–662, 1998.

Barnes, J. and Pfirrmann, T.: The influence of CO_2 and O_3, singly and in combination, on gas exchange, growth and nutrient status of radish (*Raphanus sativus* L.), New Phytologist, 121, 403–412, 1992.

Broadmeadow, M. S. and Jackson, S.: Growth responses of *Quercus petraea*, *Fraxinus excelsior* and *Pinus sylvestris* to elevated carbon dioxide, ozone and water supply, The New Phytologist, 146, 437–451, 2000.

Büker, P., Feng, Z., Uddling, J., Briolat, A., Alonso, R., Braun, S., Elvira, S., Gerosa, G., Karlsson, P., Le Thiec, D., Marzuoli, R., Mills, G., Oksanen, E., Wieser, G., , Wilkinson, M., and Emberson, L.: New flux based dose-response relationships for ozone for European forest tree species, Environmental Pollution, 206, 163–174, https://doi.org/10.1016/j.envpol.2015.06.033, http://tinyurl.sfx.mpg.de/ug3q, 2015.

Cailleret, M., Ferretti, M., Gessler, A., Rigling, A., and Schaub, M.: Ozone effects on European forest growth—Towards an integrative approach, Journal of Ecology, 106, 1377–1389, 2018.

Cionni, I., Eyring, V., Lamarque, J.-F., Randel, W., Stevenson, D., Wu, F., Bodeker, G., Shepherd, T., Shindell, D., and Waugh, D.: Ozone database in support of CMIP5 simulations: results and corresponding radiative forcing, Atmospheric Chemistry and Physics, 11, 11 267–11 292, 2011.

Cooper, O. R., Parrish, D., Ziemke, J., Balashov, N., Cupeiro, M., Galbally, I., Gilge, S., Horowitz, L., Jensen, N., Lamarque, J.-F., Naik, V., Oltmans, S., Schwab, J., Shindell, D., Thompson, A., Thouret, V., Wang, Y., and Zbinden, R.: Global distribution and trends of tropospheric ozone: An observation-based review, Elementa: Science of the Anthropocene, 2, 000 029, https://doi.org/10.12952/journal.elementa.000029, 2014.

Dufresne, J.-L., Foujols, M.-A., Denvil, S., Caubel, A., Marti, O., Aumont, O., Balkanski, Y., Bekki, S., Bellenger, H., Benshila, R., Bony, S., Bopp, L., Braconnot, P., Brockmann, P., Cadule, P., Cheruy, F., Codron, F., Cozic, A., Cugnet, D., de Noblet, N., Duvel, J.-P., Ethé, C., Fairhead, L., Fichefet, T., Flavoni, S., Friedlingstein, P., Grandpeix, J.-Y., Guez, L., Guilyardi, E., Hauglustaine, D., Hourdin, F., Idelkadi, A., Ghattas, J., Joussaume, S., Kageyama, M., Krinner, G., Labetoulle, S., Lahellec, A., Lefebvre, M.-P., Lefevre, F., Levy, C., Li, Z. X., Lloyd, J., Lott, F., Madec, G., Mancip, M., Marchand, M., Masson, S., Meurdesoif, Y., Mignot, J., Musat, I., Parouty, S., Polcher, J., Rio, C., Schulz, M., Swingedouw, D., Szopa, S., Talandier, C., Terray, P., Viovy, N., and Vuichard, N.: Climate change projections using the IPSL-CM5 Earth System Model: from CMIP3 to CMIP5, Climate Dynamics, 40, 2123–2165, 2013.

Felzer, B., Kicklighter, D., Melillo, J., Wang, C., Zhuang, Q., and Prinn, R.: Effects of ozone on net primary production and carbon sequestration in the conterminous United States using a biogeochemistry model, Tellus B, 56, 230–248, 2004.

Felzer, B., Reilly, J., Melillo, J., Kicklighter, D., Sarofim, M., Wang, C., Prinn, R., and Zhuang, Q.: Future Effects of Ozone on Carbon Sequestration and Climate Change Policy Using a Global Biogeochemical Model, Climatic Change, 73, 345–373, 2005.

Feng, Z. and Kobayashi, K.: Assessing the impacts of current and future concentrations of surface ozone on crop yield with meta-analysis, Atmospheric Environment, 43, 1510–1519, 2009.

Fiscus, E., Booker, F., and Burkey, K.: Crop responses to ozone: uptake, modes of action, carbon assimilation and partitioning, Plant, Cell & Environment, 28, 997–1011, 2005.

Franz, M., Simpson, D., Arneth, A., and Zaehle, S.: Development and evaluation of an ozone deposition scheme for coupling to a terrestrial biosphere model, Biogeosciences, 14, 45–71, https://doi.org/10.5194/bg-14-45-2017, http://www.biogeosciences.net/14/45/2017/, 2017.

Franz, M., Alonso, R., Arneth, A., Büker, P., Elvira, S., Gerosa, G., Emberson, L., Feng, Z., Le Thiec, D., Marzuoli, R., Oksanen, E., Uddling, J., Wilkinson, M., and Zaehle, S.: Evaluation of simulated ozone effects in forest ecosystems against biomass damage estimates from fumigation experiments, Biogeosciences, 15, 6941–6957, https://doi.org/10.5194/bg-15-6941-2018, https://www.biogeosciences.net/15/6941/2018/, 2018.

Friend, A.: Modelling canopy CO_2 fluxes: are 'big-leaf'simplifications justified?, Global Ecology and Biogeography, 10, 603–619, 2001.

Fusco, A. and Logan, J.: Analysis of 1970–1995 trends in tropospheric ozone at Northern Hemisphere midlatitudes with the GEOS-CHEM model, J. Geophys. Res, 108, 1988–1997, 2003.

Galloway, J. N., Dentener, F. J., Capone, D. G., Boyer, E. W., Howarth, R. W., Seitzinger, S. P., Asner, G. P., Cleveland, C. C., Green, P., Holland, E. A., Karl, D., Michaels, A., Porter, J., Townsend, A., and Vöosmarty, C.: Nitrogen Cycles: Past, Present, and Future, Biogeochemistry, 70, 153–226, 2004.

Grantz, D., Gunn, S., and VU, H.: O_3 impacts on plant development: a meta-analysis of root/shoot allocation and growth, Plant, Cell & Environment, 29, 1193–1209, 2006.

Hayes, F., Jones, M., Mills, G., and Ashmore, M.: Meta-analysis of the relative sensitivity of semi-natural vegetation species to ozone, Environmental Pollution, 146, 754–762, 2007.

Hempel, S., Frieler, K., Warszawski, L., Schewe, J., and Piontek, F.: A trend-preserving bias correction–the ISI-MIP approach, Earth System Dynamics, 4, 219–236, 2013.

Hurtt, G. C., Chini, L. P., Frolking, S., Betts, R. A., Feddema, J., Fischer, G., Fisk, J. P., Hibbard, K., Houghton, R. A., Janetos, A., Jones, C. D., Kindermann, G., Kinoshita, T., Klein Goldewijk, K., Riahi, K., Shevliakova, E., Smith, S., Stehfest, E., Thomson, A., Thornton, P., van Vuuren, D. P., and Wang, Y. P.: Harmonization of land-use scenarios for the period 1500–2100: 600 years of global gridded annual land-use transitions, wood harvest, and resulting secondary lands, Climatic Change, 109, 117, https://doi.org/10.1007/s10584-011-0153-2, https://doi.org/10.1007/s10584-011-0153-2, 2011.

Isebrands, J., McDonald, E., Kruger, E., Hendrey, G., Percy, K., Pregitzer, K., Sober, J., and Karnosky, D.: Growth responses of *Populus tremuloides* clones to interacting elevated carbon dioxide and tropospheric ozone, Environmental Pollution, 115, 359–371, 2001.

Kangasjärvi, J., Talvinen, J., Utriainen, M., and Karjalainen, R.: Plant defence systems induced by ozone, Plant, Cell & Environment, 17, 783–794, 1994.

Karnosky, D. F., Zak, D. R., Pregitzer, K. S., Awmack, C. S., Bockheim, J. G., Dickson, R. E., Hendrey, G. R., Host, G. E., King, J. S., Kopper, B. J., Kruger, E. L., Kubiske, M. E., Lindroth, R. L., Mattson, W. J., Mcdonald, E. P., Noormets, A., Oksanen, E., Parsons, W. F. J., Percy, K. E., Podila, G. K., Riemenschneider, D. E., Sharma, P., Thakur, R., Sôber, A., Sôber, J., Jones, W. S., Anttonen, S., Vapaavuori, E., Mankovska, B., Heilman, W., and Isebrands, J. G.: Tropospheric O_3 moderates responses of temperate hardwood forests to elevated CO_2: a synthesis of molecular to ecosystem results from the Aspen FACE project, Functional Ecology, 17, 289–304, 2003.

King, J., Kubiske, M., Pregitzer, K., Hendrey, G., McDonald, E., Giardina, C., Quinn, V., and Karnosky, D.: Tropospheric O_3 compromises net primary production in young stands of trembling aspen, paper birch and sugar maple in response to elevated atmospheric CO_2, New Phytologist, 168, 623–636, 2005.

Klingberg, J., Engardt, M., Karlsson, P., Langner, J., and Pleijel, H.: Declining risk of ozone impacts on vegetation in Europe 1990–2050 due to reduced precursor emissions in a changed climate, Biogeosciences Discussions, 11, 625–655, 2014.

Kozovits, A. R., Matyssek, R., Blaschke, H., Göttlein, A., and Grams, T. E.: Competition increasingly dominates the responsiveness of juvenile beech and spruce to elevated CO_2 and/or O_3 concentrations throughout two subsequent growing seasons, Global Change Biology, 11, 1387–1401, 2005.

Krinner, G., Viovy, N., de Noblet-Ducoudré, N., Ogée, J., Polcher, J., Friedlingstein, P., Ciais, P., Sitch, S., and Prentice, I.: A dynamic global vegetation model for studies of the coupled atmosphere-biosphere system, Global Biogeochemical Cycles, 19, GB1015, https://doi.org/10.1029/2003GB002199, 2005.

Kronfuß, G., Polle, A., Tausz, M., Havranek, W., and Wieser, G.: Effects of ozone and mild drought stress on gas exchange, antioxidants and chloroplast pigments in current-year needles of young Norway spruce [*Picea abies* (L.) Karst.], Trees-Structure and Function, 12, 482–489, 1998.

Kubiske, M., Quinn, V., Marquardt, P., and Karnosky, D.: Effects of Elevated Atmospheric CO_2 and/or O_3 on Intra-and Interspecific Competitive Ability of Aspen, Plant Biology, 9, 342–355, 2007.

Kull, O. and Kruijt, B.: Leaf photosynthetic light response: a mechanistic model for scaling photosynthesis to leaves and canopies, Functional Ecology, 12, 767–777, 1998.

Laisk, A., Kull, O., and Moldau, H.: Ozone Concentration in Leaf Intercellular Air Spaces is Close to Zero, Plant Physiology, 90, 1163–1167, 1989.

Lamarque, J. F., Bond, T. C., Eyring, V., Granier, C., Heil, A., Klimont, Z., Lee, D., Liousse, C., Mieville, A., Owen, B., Schultz, M. G., Shindell, D., Smith, S. J., Stehfest, E., Van Aardenne, J., Cooper, O. R., Kainuma, M., Mahowald, N., McConnell, J. R., Naik, V., Riahi, K., and van Vuuren, D. P.: Historical (1850-2000) gridded anthropogenic and biomass burning emissions of reactive gases and aerosols: methodology and application, Atmos. Chem. Physics, 10, 7017–7039, https://doi.org/10.5194/acp-10-7017-2010, 2010.

Lamarque, J.-F., Dentener, F., McConnell, J., Ro, C.-U., Shaw, M., Vet, R., Bergmann, D., Cameron-Smith, P., Dalsoren, S., Doherty, R., Faluvegi, G., Ghan, S. J., Josse, B., Lee, Y. H., MacKenzie, I. A., Plummer, D., Shindell, D. T., Skeie, R. B., Stevenson, D. S., Strode, S., Zeng, G., Curran, M., Dahl-Jensen, D., Das, S., Fritzsche, D., and Nolan, M.: Multi-model mean nitrogen and sulfur deposition from the Atmospheric Chemistry and Climate Model Intercomparison Project (ACCMIP): evaluation of historical and projected future changes, Atmospheric Chemistry and Physics, 13, 7997–8018, https://doi.org/10.5194/acp-13-7997-2013, https://acp.copernicus.org/articles/13/7997/2013/, 2013.

Langebartels, C., Kerner, K., Leonardi, S., Schraudner, M., Trost, M., Heller, W., and Sandermann Jr, H.: Biochemical Plant Responses to Ozone: I. Differential Induction of Polyamine and Ethylene Biosynthesis in Tobacco, Plant Physiology, 95, 882, 1991.

LeBauer, D. and Treseder, K.: Nitrogen limitation of net primary productivity in terrestrial ecosystems is globally distributed, Ecology, 89, 371–379, 2008.

Leisner, C. and Ainsworth, E.: Quantifying the effects of ozone on plant reproductive growth and development, Global Change Biology, 18, 606–616, 2012.

Li, P., Feng, Z., Catalayud, V., Yuan, X., Xu, Y., and Paoletti, E.: A meta-analysis on growth, physiological and biochemical responses of woody species to ground-level ozone highlights the role of plant functional types, Plant, Cell & Environment, 40, 2369–2380, 2017.

Lombardozzi, D., Levis, S., Bonan, G., and Sparks, J.: Predicting photosynthesis and transpiration responses to ozone: decoupling modeled photosynthesis and stomatal conductance, Biogeosciences, 9, 3113–3130, 2012.

Lombardozzi, D., Sparks, J. P., and Bonan, G.: Integrating O_3 influences on terrestrial processes: photosynthetic and stomatal response data available for regional and global modeling, Biogeosciences, 10, 6815–6831, https://doi.org/10.5194/bgd-10-6973-2013, http://www.biogeosciences-discuss.net/10/6973/2013/, 2013.

Lombardozzi, D., Levis, S., Bonan, G., Hess, P., and Sparks, J.: The Influence of Chronic Ozone Exposure on Global Carbon and Water Cycles, Journal of Climate, 28, 292–305, 2015.

LRTAP-Convention: Manual on Methodologies and Criteria for Modelling and Mapping Critical Loads and Levels; and Air Pollution Effects, Risks and Trends, https://icpvegetation.ceh.ac.uk/, https://icpvegetation.ceh.ac.uk/publications/documents/FinalnewChapter3v4Oct2017_000.pdf, 2017.

Marenco, A., Gouget, H., Nédélec, P., Pagés, J., and Karcher, F.: Evidence of a long-term increase in tropospheric ozone from Pic du Midi data series: Consequences: Positive radiative forcing, Journal of Geophysical Research: Atmospheres (1984–2012), 99, 16 617–16 632, 1994.

Massman, W.: A review of the molecular diffusivities of H_2O, CO_2, CH_4, CO, O_3, SO_2, NH_3, N_2O, NO, and NO_2 in air, O_2 and N_2 near STP, Atmospheric Environment, 32, 1111–1127, https://doi.org/10.1016/S1352-2310(97)00391-9, http://tinyurl.sfx.mpg.de/ucen, 1998.

McAinsh, M., Evans, N., Montgomery, L., and North, K.: Calcium signalling in stomatal responses to pollutants, New Phytologist, 153, 441–447, 2002.

Medlyn, B., Barton, C., Broadmeadow, M., Ceulemans, R., De Angelis, P., Forstreuter, M., Freeman, M., Jackson, S., Kellomäki, S., Laitat, E., et al.: Stomatal conductance of forest species after long-term exposure to elevated CO_2 concentration: A synthesis, New Phytologist, 149, 247–264, 2001.

Meinshausen, M., Smith, S. J., Calvin, K., Daniel, J. S., Kainuma, M., Lamarque, J.-F., Matsumoto, K., Montzka, S., Raper, S., Riahi, K., Thomson, A., Velders, G. J. M., and van Vuuren, D. P.: The RCP greenhouse gas concentrations and their extensions from 1765 to 2300, Climatic Change, 109, 213, 2011.

Meleux, F., Solmon, F., and Giorgi, F.: Increase in summer European ozone amounts due to climate change, Atmospheric Environment, 41, 7577–7587, 2007.

Meyerholt, J. and Zaehle, S.: The role of stoichiometric flexibility in modelling forest ecosystem responses to nitrogen fertilization, New Phytologist, 208, 1042–1055, https://doi.org/10.1111/nph.13547, https://nph.onlinelibrary.wiley.com/doi/abs/10.1111/nph.13547, 2015.

Moss, R. H., Edmonds, J. A., Hibbard, K. A., Manning, M. R., Rose, S. K., Van Vuuren, D. P., Carter, T. R., Emori, S., Kainuma, M., Kram, T., Meehl, G. A., Mitchell, J. F. B., Nakicenovic, N., Riahi, K., Smith, S. J., Stouffer, R. J., Thomson, A. M., Weyant, J. P., and Wilbanks, T. J.: The next generation of scenarios for climate change research and assessment, Nature, 463, 747, 2010.

Niinemets, Ü., Keenan, T. F., and Hallik, L.: A worldwide analysis of within-canopy variations in leaf structural, chemical and physiological traits across plant functional types, New Phytologist, 205, 973–993, 2015.

Noormets, A., Sober, A., Pell, E., Dickson, R., Podila, G., Sober, J., Isebrands, J., and Karnosky, D.: Stomatal and non-stomatal limitation to photosynthesis in two trembling aspen (*Populus tremuloides* Michx.) clones exposed to elevated CO_2 and/or O_3, Plant, Cell & Environment, 24, 327–336, 2001.

Noormets, A., Kull, O., Sôber, A., Kubiske, M., and Karnosky, D.: Elevated CO_2 response of photosynthesis depends on ozone concentration in aspen, Environmental Pollution, 158, 992–999, 2010.

Norby, R.: Nitrogen deposition: a component of global change analyses, New Phytologist, 139, 189–200, 1998.

Norby, R., Warren, J., Iversen, C., Garten, C., Medlyn, B., and McMurtrie, R.: CO_2 Enhancement of Forest Productivity Constrained by Limited Nitrogen Availability, Nature Precedings, https://doi.org/10.1038/npre.2009.3747.1, 2009.

Oliver, R. J., Mercado, L. M., Sitch, S., Simpson, D., Medlyn, B. E., Lin, Y.-S., and Folberth, G. A.: Large but decreasing effect of ozone on the European carbon sink, Biogeosciences, 15, 4245–4269, 2018.

Oren, R., Ellsworth, D. S., Johnsen, K. H., Phillips, N., Ewers, B. E., Maier, C., Schäfer, K. V., McCarthy, H., Hendrey, G., McNulty, S. G., and Katul, G. G.: Soil fertility limits carbon sequestration by forest ecosystems in a CO2-enriched atmosphere, Nature, pp. 469–472, https://doi.org/10.1038/35078064, 2001.

Paoletti, E. and Grulke, N.: Does living in elevated CO_2 ameliorate tree response to ozone? A review on stomatal responses, Environmental Pollution, 137, 483–493, 2005.

Quéré, C. L., Andrew, R. M., Friedlingstein, P., Sitch, S., Hauck, J., Pongratz, J., Pickers, P. A., Korsbakken, J. I., Peters, G. P., Canadell, J. G., Arneth, A., Arora, V. K., Barbero, L., Bastos, A., Bopp, L., Chevallier, F., Chini, L. P., Ciais, P., Doney, S. C., Gkritzalis, T., Goll, D. S., Harris, I., Haverd, V., Hoffman, F. M., Hoppema, M., Houghton, R. A., Hurtt, G., Ilyina, T., Jain, A. K., Johannessen, T., Jones, C. D., Kato, E., Keeling, R. F., Goldewijk, K. K., Landschützer, P., Lefèvre, N., Lienert, S., Liu, Z., Lombardozzi, D., Metzl, N., Munro, D. R., Nabel, J. E. M. S., ichiro Nakaoka, S., Neill, C., Olsen, A., Ono, T., Patra, P., Peregon, A., Peters, W., Peylin, P., Pfeil, B., Pierrot, D., Poulter, B., Rehder, G., Resplandy, L., Robertson, E., Rocher, M., Rödenbeck, C., Schuster, U., Schwinger, J., Séférian, R., Skjelvan, I., Steinhoff, T., Sutton, A., Tans, P. P., Tian, H., Tilbrook, B., Tubiello, F. N., van der Laan-Luijkx, I. T., van der Werf, G. R., Viovy, N., Walker, A. P., Wiltshire, A. J., Wright, R., Zaehle, S., and Zheng, B.: Global Carbon Budget 2018, Earth System Science Data, 10, 2141–2194, https://doi.org/10.5194/essd-10-2141-2018, https://ueaeprints.uea.ac.uk/id/eprint/69293/, 2018.

Ren, W., Tian, H., Liu, M., Zhang, C., Chen, G., Pan, S., Felzer, B., and Xu, X.: Effects of tropospheric ozone pollution on net primary productivity and carbon storage in terrestrial ecosystems of China, Journal of Geophysical Research: Atmospheres, 112, 2007.

Ren, W., Tian, H., Tao, B., Chappelka, A., Sun, G., Lu, C., Liu, M., Chen, G., and Xu, X.: Impacts of tropospheric ozone and climate change on net primary productivity and net carbon exchange of China's forest ecosystems, Global Ecology and Biogeography, 20, 391–406, 2011.

Riikonen, J., Lindsberg, M.-M., Holopainen, T., Oksanen, E., Lappi, J., Peltonen, P., and Vapaavuori, E.: Silver birch and climate change: variable growth and carbon allocation responses to elevated concentrations of carbon dioxide and ozone, Tree Physiology, 24, 1227–1237, 2004.

Sanz, M., Calatayud, V., and Sánchez-Peña, G.: Measures of ozone concentrations using passive sampling in forests of South Western Europe, Environmental Pollution, 145, 620–628, 2007.

Schaub, M., Skelly, J., Zhang, J., Ferdinand, J., Savage, J., Stevenson, R., Davis, D., and Steiner, K.: Physiological and foliar symptom response in the crowns of *Prunus serotina*, *Fraxinus americana* and *Acer rubrum* canopy trees to ambient ozone under forest conditions, Environmental Pollution, 133, 553–567, 2005.

Schulte-Uebbing, L. and de Vries, W.: Global-scale impacts of nitrogen deposition on tree carbon sequestration in tropical, temperate, and boreal forests: A meta-analysis, Global Change Biology, 24, e416–e431, https://doi.org/https://doi.org/10.1111/gcb.13862, https://onlinelibrary.wiley.com/doi/abs/10.1111/gcb.13862, 2018.

Sicard, P., Anav, A., Marco, A. D., and Paoletti, E.: Projected global ground-level ozone impacts on vegetation under different emission and climate scenarios, Atmospheric Chemistry and Physics, 17, 12 177–12 196, 2017.

Sitch, S., Cox, P., Collins, W., and Huntingford, C.: Indirect radiative forcing of climate change through ozone effects on the land-carbon sink, Nature, 448, 791–794, 2007.

Staehelin, J., Thudium, J., Buehler, R., Volz-Thomas, A., and Graber, W.: Trends in surface ozone concentrations at Arosa (Switzerland), Atmospheric Environment, 28, 75–87, 1994.

Talhelm, A. F., Pregitzer, K. S., Kubiske, M. E., Zak, D. R., Campany, C. E., Burton, A. J., Dickson, R. E., Hendrey, G. R., Isebrands, J. G., Lewin, K. F., Nagy, J., and Karnosky, D. F.: Elevated carbon dioxide and ozone alter productivity and ecosystem carbon content in northern temperate forests, Global Change Biology, 20, 2492–2504, https://doi.org/10.1111/gcb.12564, https://onlinelibrary.wiley.com/doi/abs/10.1111/gcb.12564, 2014.

Tausz, M., Grulke, N., and Wieser, G.: Defense and avoidance of ozone under global change, Environmental Pollution, 147, 525–531, 2007.

Thomas, R. Q., Canham, C. D., Weathers, K. C., and Goodale, C. L.: Increased tree carbon storage in response to nitrogen deposition in the US, Nature Geoscience, 3, 13–17, 2010.

Tjoelker, M., Volin, J., Oleksyn, J., and Reich, P.: Interaction of ozone pollution and light effects on photosynthesis in a forest canopy experiment, Plant, Cell & Environment, 18, 895–905, 1995.

Turnock, S. T., Allen, R. J., Andrews, M., Bauer, S. E., Deushi, M., Emmons, L., Good, P., Horowitz, L., John, J. G., Michou, M., Nabat, P., Naik, V., Neubauer, D., O'Connor, F. M., Olivié, D., Oshima, N., Schulz, M., Sellar, A., Shim, S., Takemura, T., Tilmes, S., Tsigaridis, K., Wu, T., and Zhang, J.: Historical and future changes in air pollutants from CMIP6 models, Atmospheric Chemistry and Physics, 20, 14 547–14 579, https://doi.org/10.5194/acp-20-14547-2020, https://acp.copernicus.org/articles/20/14547/2020/, 2020.

Uddling, J., Hogg, A., Teclaw, R., Carroll, M., and Ellsworth, D.: Stomatal uptake of O_3 in aspen and aspen-birch forests under free-air CO_2 and O_3 enrichment, Environmental Pollution, 158, 2023–2031, 2010.

van Vuuren, D. P., Edmonds, J., Kainuma, M., Riahi, K., Thomson, A., Hibbard, K., Hurtt, G. C., Kram, T., Krey, V., Lamarque, J.-F., Masui, T., Meinshausen, M., Nakicenovic, N., Smith, S. J., and Rose, S. K.: The representative concentration pathways: an overview, Climatic Change, 109, 5, https://doi.org/10.1007/s10584-011-0148-z, https://doi.org/10.1007/s10584-011-0148-z, 2011.

Vitousek, P. M. and Howarth, R. W.: Nitrogen limitation on land and in the sea: how can it occur?, Biogeochemistry, 13, 87–115, 1991.

Wang, B., Shugart, H. H., Shuman, J. K., and Lerdau, M. T.: Forests and ozone: productivity, carbon storage, and feedbacks, Scientific Reports, 6, 22 133, 2016.

Wang, R., Goll, D., Balkanski, Y., Hauglustaine, D., Boucher, O., Ciais, P., Janssens, I., Penuelas, J., Guenet, B., Sardans, J., Bopp, L., Vuichard, N., Zhou, F., Li, B., Piao, S., Peng, S., Huang, Y., and Tao, S.: Global forest carbon uptake due to nitrogen and phosphorus deposition from 1850 to 2100, Global Change Biology, 23, 4854–4872, https://doi.org/https://doi.org/10.1111/gcb.13766, https://onlinelibrary.wiley.com/doi/abs/10.1111/gcb.13766, 2017.

Wild, O., Fiore, A. M., Shindell, D., Doherty, R., Collins, W., Dentener, F., Schultz, M., Gong, S., MacKenzie, I., Zeng, G., Hess, P., Duncan, B. N., Bergmann, D. J., Szopa, S., Jonson, J. E., Keating, T. J., and Zuber, A.: Modelling future changes in surface ozone: a parameterized approach, Atmospheric Chemistry and Physics, 12, 2037–2054, 2012.

Wittig, V., Ainsworth, E., and Long, S.: To what extent do current and projected increases in surface ozone affect photosynthesis and stomatal conductance of trees? A meta-analytic review of the last 3 decades of experiments, Plant, Cell & Environment, 30, 1150–1162, 2007.

Wittig, V., Ainsworth, E., Naidu, S., Karnosky, D., and Long, S.: Quantifying the impact of current and future tropospheric ozone on tree biomass, growth, physiology and biochemistry: a quantitative meta-analysis, Global Change Biology, 15, 396–424, 2009.

Wohlgemuth, H., Mittelstrass, K., Kschieschan, S., Bender, J., Weigel, H., Overmyer, K., Kangasjärvi, J., Sandermann, H., and Langebartels, C.: Activation of an oxidative burst is a general feature of sensitive plants exposed to the air pollutant ozone, Plant, Cell & Environment, 25, 717–726, 2002.

Wustman, B., Oksanen, E., Karnosky, D., Noormets, A., Isebrands, J., Pregitzer, K., Hendrey, G., Sober, J., and Podila, G.: Effects of elevated CO_2 and O_3 on aspen clones varying in O_3 sensitivity: can CO_2 ameliorate the harmful effects of O_3?, Environmental Pollution, 115, 473–481, 2001.

Yue, X. and Unger, N.: Ozone vegetation damage effects on gross primary productivity in the United States, Atmospheric Chemistry and Physics, 14, 9137–9153, 2014.

Zaehle, S.: Terrestrial nitrogen–carbon cycle interactions at the global scale, Philosophical Transactions of the Royal Society B: Biological Sciences, 368, 20130 125, https://doi.org/10.1098/rstb.2013.0125, https://royalsocietypublishing.org/doi/abs/10.1098/rstb.2013.0125, 2013.

Zaehle, S. and Friend, A.: Carbon and nitrogen cycle dynamics in the O-CN land surface model: 1. Model description, site-scale evaluation, and sensitivity to parameter estimates, Global Biogeochemical Cycles, 24, GB1005, http://dx.doi.org/10.1029/2009GB003521, 2010.

Zaehle, S., Friend, A., Friedlingstein, P., Dentener, F., Peylin, P., and Schulz, M.: Carbon and nitrogen cycle dynamics in the O-CN land surface model: 2. Role of the nitrogen cycle in the historical terrestrial carbon balance, Global Biogeochemical Cycles, 24, GB1006, 2010.

Zaehle, S., Ciais, P., Friend, A. D., and Prieur, V.: Carbon benefits of anthropogenic reactive nitrogen offset by nitrous oxide emissions, Nature Geoscience, 4, 601–605, 2011.

Zaehle, S., Medlyn, B. E., De Kauwe, M. G., Walker, A. P., Dietze, M. C., Hickler, T., Luo, Y., Wang, Y.-P., El-Masri, B., Thornton, P., Jain, A., Wang, S., Warlind, D., Weng, E., Parton, W., Iversen, C. M., Gallet-Budynek, A., McCarthy, H., Finzi, A., Hanson, P. J., Prentice, I. C., Oren, R., and Norby, R. J.: Evaluation of 11 terrestrial carbon–nitrogen cycle models against observations from two temperate Free-Air CO2 Enrichment studies, New Phytologist, 202, 803–822, https://doi.org/10.1111/nph.12697, https://nph.onlinelibrary.wiley.com/doi/abs/10.1111/nph.12697, 2014.

Zak, D. R., Pregitzer, K. S., Kubiske, M. E., and Burton, A. J.: Forest productivity under elevated CO_2 and O_3: positive feedbacks to soil N cycling sustain decade-long net primary productivity enhancement by CO_2, Ecology Letters, 14, 1220–1226, 2011.

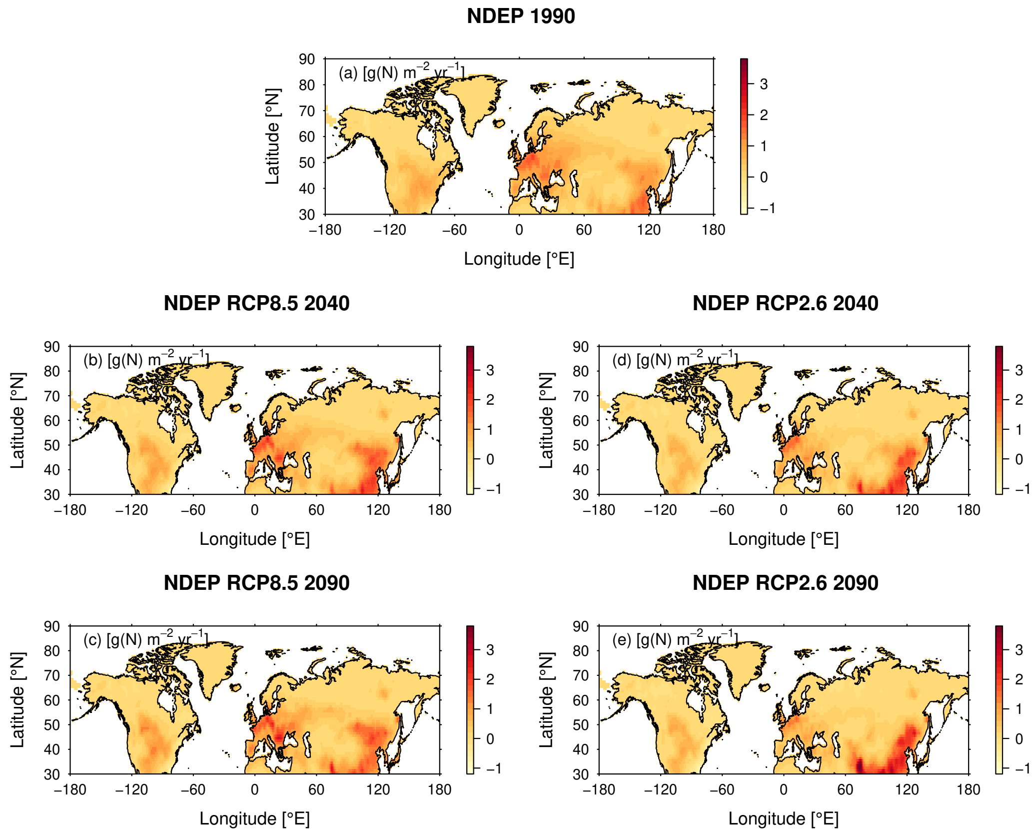

Figure S1. Mean simulated change in nitrogen deposition rates for the temperate and boreal Northern Hemisphere ($\geq 30°$N) in the decades of the years of 1990, 2040 and 2090 compared to the decade of the year 1850, each according to the RCP2.6 and RCP8.5 ~~pollution~~ emission scenario.

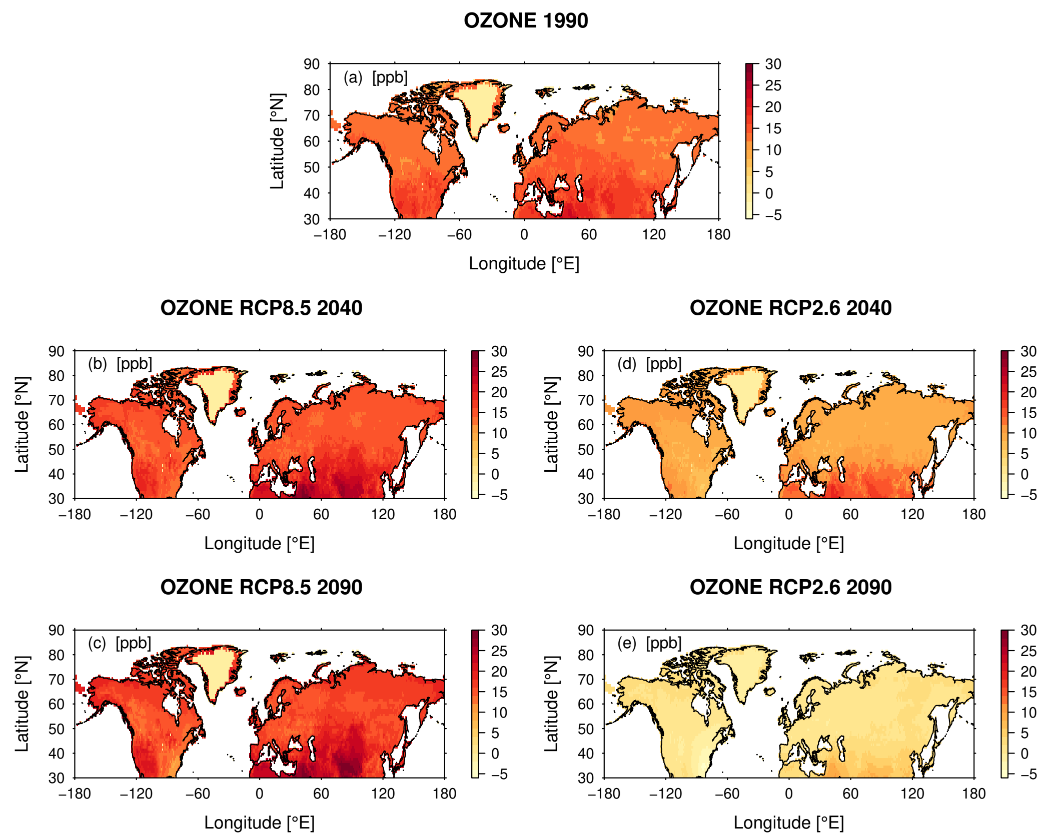

Figure S2. Mean simulated change in canopy level O_3 concentration for the temperate and boreal Northern Hemisphere ($\geq 30°$N) in the decades of the years of 1850, 1990, 2040 and 2090 compared to the decade of the year 1850, each according to the RCP2.6 and RCP8.5 ~~pollution~~ emission scenario.

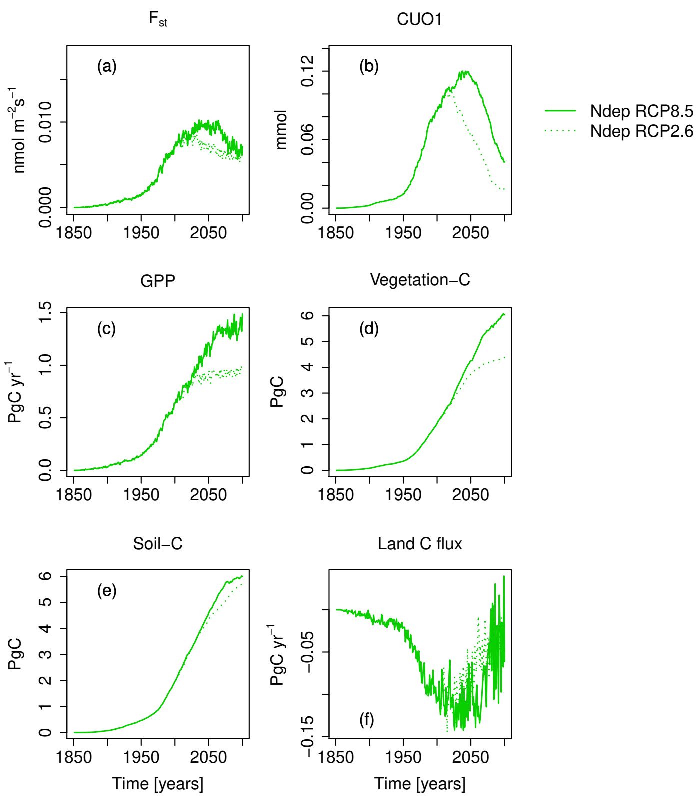

Figure S3. Nitrogen deposition induced absolute change in regional mean ~~ozone~~ O_3 uptake (F_{st}), mean cumulative O_3 uptake above a flux threshold of $1\ \mathrm{nmol\,m^{-2}\,s^{-1}}$ (CUO1), summed GPP, ~~summed~~ total carbon biomass in vegetation (vegetation-C), summed carbon soil organic matter (soil-C), and summed land carbon flux (land C flux) compared to pre-industrial values in the simulation region. The nitrogen deposition induced change is calculated from the simulation runs S3 and S5 (see Tab. 2). Solid lines indicate results from simulations based on RCP8.5, dotted lines results from simulations based on RCP2.6. The effect of the seasonal cycle is smoothed by the application of a moving average of 12 months (a,b).

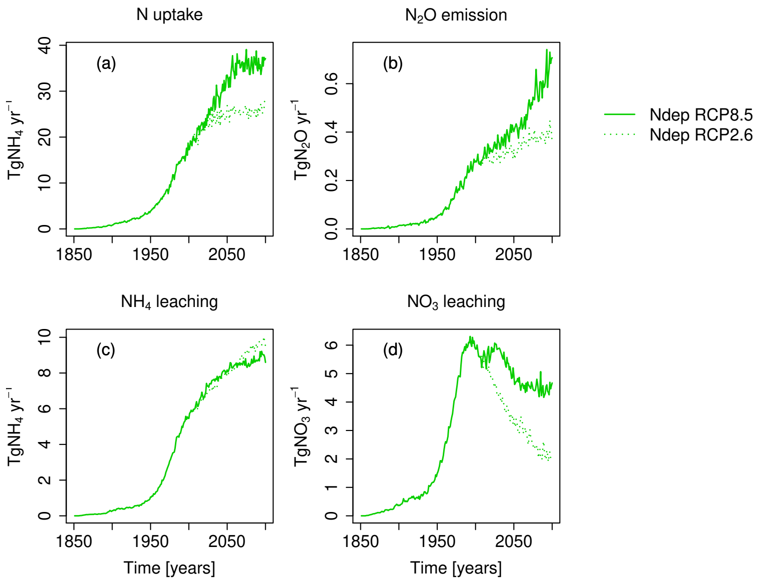

Figure S4. Nitrogen deposition induced absolute change in ~~regional summed~~ total N uptake by region, N_2O emission, NH_4 leaching and N_2O leaching compared to pre-industrial values in the simulation region. The nitrogen deposition induced absolute change is calculated from the simulation runs S3 and S5 (see Tab. 2). Solid lines indicate results from simulations based on RCP8.5, dotted lines results from simulations based on RCP2.6.

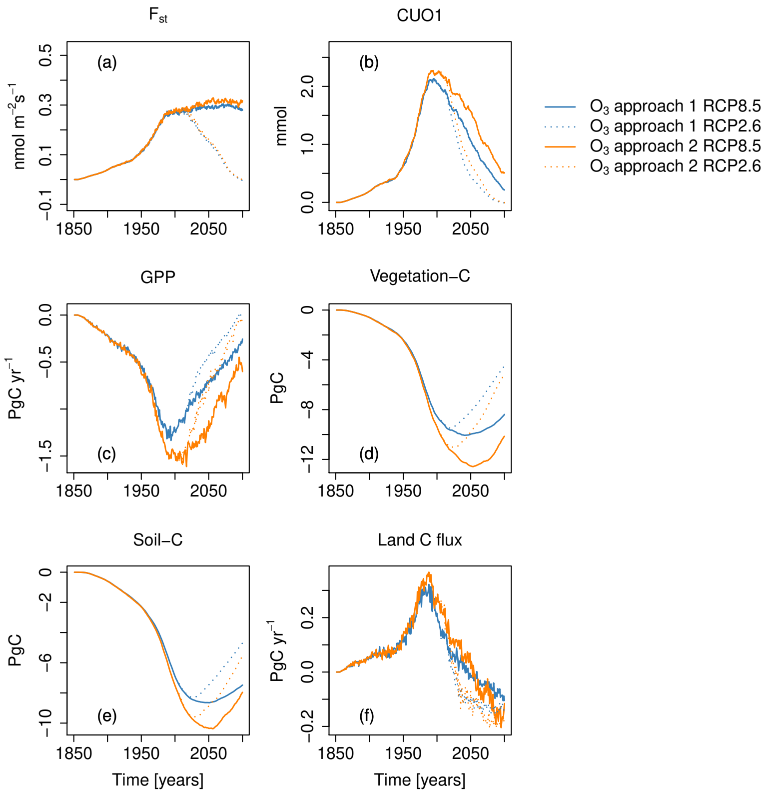

Figure S5. Ozone induced absolute change in regional mean ~~ozone~~ O_3 uptake (F_{st}), mean cumulative O_3 uptake above a flux threshold of $1\,\mathrm{nmol\,m^{-2}\,s^{-1}}$ (CUO1), summed GPP, ~~summed~~ total carbon biomass in vegetation (vegetation-C) and summed carbon soil organic matter (soil-C) compared to pre-industrial values in the simulation region. Different colors indicate different approaches to calculate the ~~ozone~~ O_3 induced change from the factorial runs. Orange lines represent approach 1: (S2-S1)/S1, blue lines approach 2:(S5-S4)/S4. Solid lines indicate results from simulations based on RCP8.5, dotted lines results from simulations based on RCP2.6. The effect of the seasonal cycle is smoothed by the application of a moving average of 12 months.

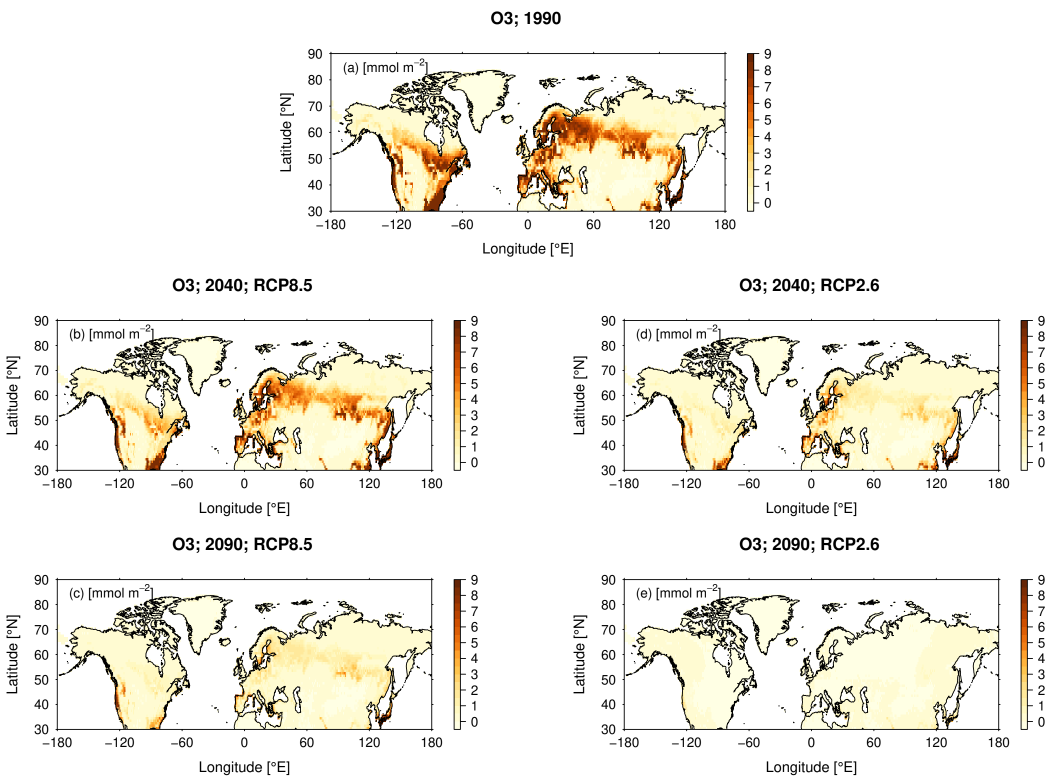

Figure S6. Absolute change in CUO1 compared to pre-industrial values induced by ~~ozone~~O_3, calculated according to approach 2. Displayed are the decade 1990 (mean of the years 1990-1999), 2040 (mean of the years 2040-2049) and of 2090 (mean of the years 2090-2099). For the decades 2040 and 2090 results from simulations based on RCP8.5 and RCP2.6 are displayed. See Tab. 2 for details on the calculation of the ~~ozone~~ O_3 impact.

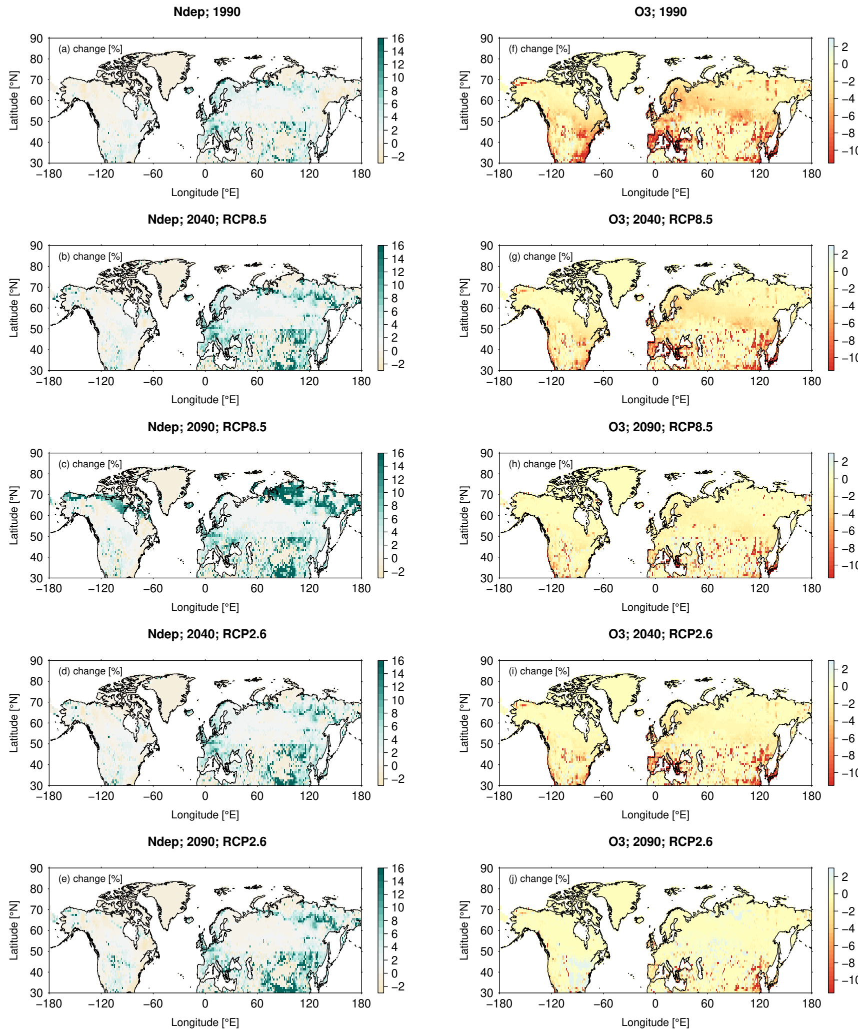

Figure S7. Relative change in GPP compared to pre-industrial values induced by nitrogen deposition (left column) and ~~ozone~~ O_3 calculated according to approach 2 (right column). The induced change in GPP is displayed for the decades 1990 (mean of the years 1990-1999), 2040 (mean of the years 2040-2049) and 2090 (mean of the years 2090-2099). For the decades 2040 and 2090 results from simulations based on RCP8.5 and RCP2.6 are displayed. See Tab. 2 for details on the calculation of the single drivers.

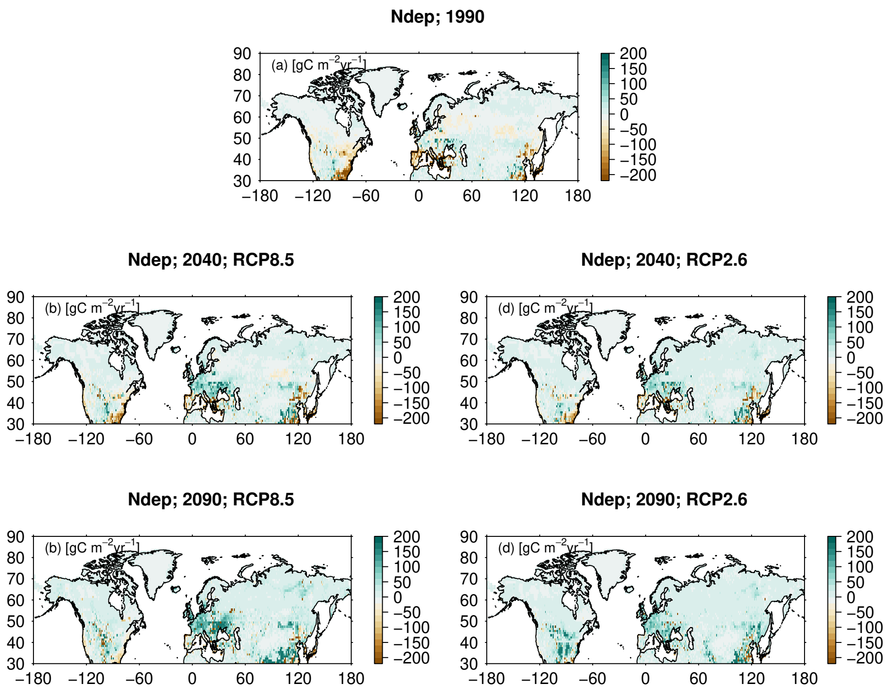

Figure S8. Combined absolute impact of nitrogen deposition and O_3 calculated according to approach 2 on GPP compared to pre-industrial values. The induced change in GPP is displayed for the decades 1990 (mean of the years 1990-1999), 2040 (mean of the years 2040-2049) and 2090 (mean of the years 2090-2099). For the decades 2040 and 2090 results from simulations based on RCP8.5 and RCP2.6 are displayed. See Tab. 2 for details on the calculation of the single drivers.

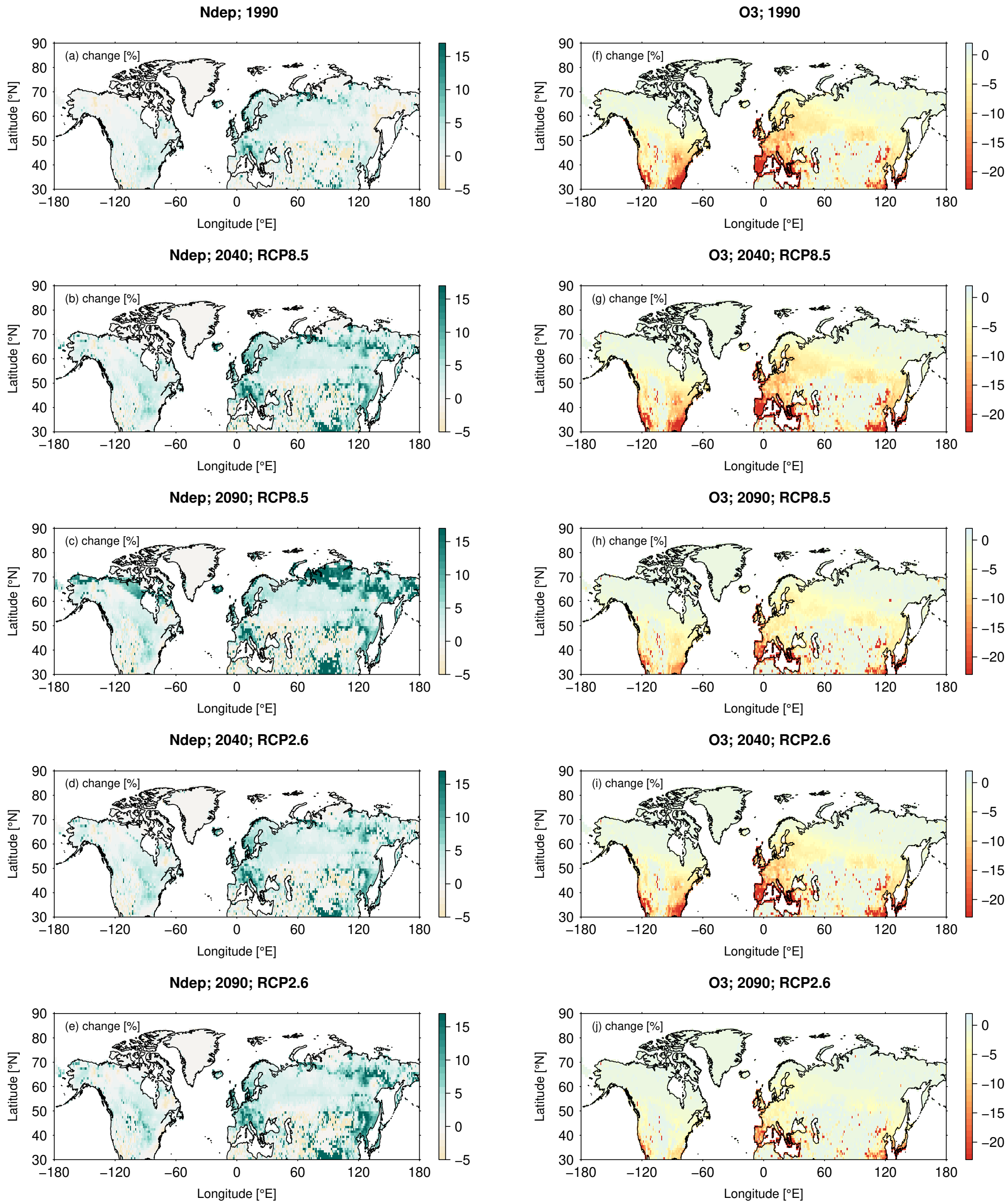

Figure S9. Relative change in the total carbon biomass in vegetation (vegetation-C) compared to pre-industrial values induced by nitrogen deposition (left column) and ~~ozone~~ O_3 calculated according to approach 2 (right column). The induced change in vegetation-C is displayed for the decades 1990 (mean of the years 1990-1999), 2040 (mean of the years 2040-2049) and 2090 (mean of the years 2090-2099). For the decades 2040 and 2090 results from simulations based on RCP8.5 and RCP2.6 are displayed. See Tab. 2 for details on the calculation of the single drivers.

Table S1. The spread in the mean percent change displayed in Tab. 4 due to inter-annual variability, derived from error propagation of the yearly estimates in GPP, total carbon biomass in vegetation (vegetation-C), and land carbon flux (land C flux) induced by O_3 during the decades of 1990 (1990–1999), 2040 (2040–2049) and 2090 (2090–2099). For O_3 two values are displayed which refer to the two approaches to calculate the O_3 impact.

Region	Pollutant	1990	2040 RCP8.5	2040 RCP2.6	2090 RCP8.5	2090 RCP2.6
GPP						
NH30	O_3	±0.17;±0.14	±0.11;±0.19	±0.09;±0.22	±0.10;±0.10	±0.10;±0.08
NH30	Ndep	±0.13	±0.18	±0.11	±0.20	±0.12
Europe	O_3	±0.25;±0.33	±0.14;±0.19	±0.14;±0.24	±0.11;±0.13	±0.04;±0.08
Europe	Ndep	±0.26	±0.30	±0.21	±0.21	±0.12
USA	O_3	±0.41;±0.39	±0.19;±0.26	±0.17;±0.30	±0.05;±0.23	±0.20;±0.17
USA	Ndep	±0.23	±0.19	±0.23	±0.30	±0.13
China	O_3	±0.95;±0.76	±0.67;±1.31	±0.45;±1.02	±0.41;±0.40	±0.43;±0.44
China	Ndep	±0.23	±0.53	±0.23	±0.40	±0.59
Vegetation-C						
NH30	O_3	±0.38;±0.40	±0.14;±0.27	±0.15;±0.17	±0.17;±0.12	±0.19;±0.18
NH30	Ndep	±0.13	±0.15	±0.09	±0.08	±0.04
Europe	O_3	±0.34;±0.42	±0.13;±0.33	±0.19;±0.21	±0.22;±0.15	±0.18;±0.24
Europe	Ndep	±0.15	±0.20	±0.11	±0.09	±0.05
USA	O_3	±0.62;±0.50	±0.26;±0.27	±0.27;±0.29	±0.16;±0.24	±0.28;±0.25
USA	Ndep	±0.10	±0.07	±0.03	±06	±0.04
China	O_3	±1.63;±1.86	±0.43;±0.60	±0.23;±0.32	±0.45;±0.44	±0.44;±0.48
China	Ndep	±0.13	±0.22	±0.19	±0.24	±0.21
Land C flux						
NH30	O_3	±4.28;±4.48	±0.78;±0.98	±2.45;±2.07	±0.88;±2.15	±3.87;±7.86
NH30	Ndep	±2.20	±1.42	±1.46	±2.04	±1.51
Europe	O_3	±12.48;±14.84	±1.19;±1.31	±3.57;±4.70	±1.45;±12.10	±8.66;±11.30
Europe	Ndep	±13.34	±2.06	±1.69	±5.06	±2.10
USA	O_3	±8.60;±12.22	±1.17;±3.20	±2.13;±6.93	±0.72;±6.25	±5.30;±12.86
USA	Ndep	±4.50	±3.85	±3.33	±4.95	±2.95
China	O_3	±13.23;±25.46	±6.35;±13.3	±6.85;±11.77	±6.64;±13.77	±16.81;±14.57
China	Ndep	±15.81	±7.00	±4.89	±6.46	±8.29